Biophysical Journal
Article

Biophysical Society

# Role of K364 next to the active site cysteine in voltage-dependent phosphatase activity of Ci-VSP

Ian Costa Paixao,[1,4] Natsuki Mizutani,[1] Makoto Matsuda,[2,3] Rizki Tsari Andriani,[1,5] Takafumi Kawai,[1] Atsushi Nakagawa,[3] Yoshifumi Okochi,[1,*] and Yasushi Okamura[1,4,*]

[1]Department of Physiology, Graduate School of Medicine, Osaka University, Suita, Japan; [2]Department Oncogene Research, Research Institute for Microbial Diseases, Osaka University, Suita, Japan; [3]Laboratory for Supramolecular Crystallography, Institute for Protein Research, Osaka University, Suita, Japan; [4]Graduate School of Frontier Biosciences, Osaka University, Suita, Japan; and [5]Graduate School of Medicine, Osaka University JSPS International Research Fellow, Suita, Japan

ABSTRACT Voltage-sensing phosphatase (VSP) consists of the voltage sensor domain (VSD) similar to that of voltage-gated ion channels and the cytoplasmic phosphatase region with remarkable similarity to the phosphatase and tensin homolog deleted on chromosome 10 (PTEN). Membrane depolarization activates VSD, leading to dephosphorylation of three species of phosphoinositides (phosphatidylinositol phosphates (PIPs)), PI(3,4,5)$P_3$, PI(4,5)$P_2$, and PI(3,4)$P_2$. VSP dephosphorylates 3- and 5-phosphate of PIPs, unlike PTEN, which shows rigid 3-phosphate specificity. In this study, a bioinformatics search showed that some mammals have VSP orthologs with amino acid diversity in the active center motif, $Cx_5R$, which is highly conserved among protein tyrosine phosphatases and PTEN-related phosphatases; lysine next to the active site cysteine in the $Cx_5R$ motif was substituted for methionine in VSP orthologs of Tasmanian devil, koala, and prairie deer mouse, and leucine in opossum. Since lysine at the corresponding site in PTEN is known to be critical for enzyme activities, we attempted to address the significance of amino acid diversity among VSP orthologs at this site. K364 was changed to different amino acids in sea squirt VSP (Ci-VSP), and voltage-dependent phosphatase activity in *Xenopus* oocyte was studied using fluorescent probes for PI(4,5)$P_2$ and PI(3,4)$P_2$. All mutants retained both 5-phosphatase and 3-phosphatase activity, indicating that lysine at this site is dispensable for 3-phosphatase activity, unlike PTEN. Notably, K364M mutant showed increased activity both of 5-phosphatase and 3-phosphatase compared with the wild type (WT). It also showed slower kinetics of voltage sensor motion. Malachite green assay of K364M mutant did not show significant difference of phosphatase activity from WT, suggesting tighter interaction between substrate binding and voltage sensing. Mutation corresponding to K364M in the zebrafish VSP led to enhanced voltage-dependent dephosphorylation of PI(4,5)$P_2$. Further studies will provide clues to understanding of substrate preference in PIPs phosphatases as well as to customization of a molecular tool.

SIGNIFICANCE As phosphoinositide phosphatase, voltage-sensing phosphatase (VSP) has two unique features: voltage-regulated enzyme activity driven by the operation of the transmembrane domain as well as dual phosphatase activities toward 3-phosphate and 5-phosphate of the inositol ring. We found that a lysine residue, one amino acid from the cysteine in the active center of the highly conserved $Cx_5R$ motif, is diversified in some mammals. This provides a clue to further understanding of mechanisms underlying substrate specificity in phosphoinositide enzymes as well as to devising a molecular tool.

## INTRODUCTION

The phosphoinositides or phosphatidylinositol phosphates (PIPs), a group of crucial lipid components of cell membrane, act as signal molecules by interacting with many types of proteins (1–5). PIPs contain seven different species of PIPs, dependent on the number and the position of their phosphate groups on the inositol ring. Subcellular localizations and density of PIPs are regulated by many types of proteins, including kinases and phosphatases.

*Submitted June 9, 2022, and accepted for publication January 18, 2023.*

*Correspondence: okochyo@phys2.med.osaka-u.ac.jp or yokamura@phys2.med.osaka-u.ac.jp

Ian Costa Paixao's present address is Department of Cell Growth and Differentiation, Center for iPS Cell Research and Application, Kyoto University, Kyoto, Japan.

Ian Costa Paixao and Natsuki Mizutani contributed equally to this work.

Editor: Valeria Vasquez.

https://doi.org/10.1016/j.bpj.2023.01.022

The voltage-sensing phosphatase (VSP) is a transmembrane phosphoinositide (PIP) phosphatase with significant sequence similarity to the phosphatase and tensin homolog deleted on chromosome 10 (PTEN). VSP consists of three distinct regions: the voltage sensor domain (VSD), which consists of four transmembrane segments (S1–S4); the linker region between the VSD and the phosphatase domain (PD); and the cytoplasmic catalytic region (CCR) with high similarity to PTEN, which consists of PD and the C2 domain (6). Unlike PTEN, which does not contain VSD, phosphatase activity of VSP toward PIPs is regulated by membrane potential change through tight coupling between VSD and the CCR (7). As another notable difference from PTEN that has 3-phosphatase activity toward $PI(3,4,5)P_3$ and $PI(3,4)P_2$, VSP shows robust 5-phosphatase activity toward $PI(4,5)P_2$ (6). Mouse VSP is expressed in sperm and plays critical role in sperm capacitation through negatively regulating $PI(4,5)P_2$-sensitive potassium channel (8). In addition, VSP has been a useful material for devising molecular tools; a genetically encoded voltage indicator and a tool for acutely reducing the level of $PI(4,5)P_2$ with electrophysiology. More than 40 species of ion channels have been studied so far for their PIPs sensitivity utilizing VSP as a tool to transiently deplete $PI(4,5)P_2$ in cells (6,9,10).

As another unique feature of the PIPs enzyme, VSP shows less rigid substrate specificity; it shows 3-phosphatase activity besides its 5-phosphatase activity. VSP mediates at least four subreactions: conversion from $PI(3,4,5)P_3$ to $PI(4,5)P_2$ and $PI(3,4)P_2$ and from $PI(3,4)P_2$ or $PI(4,5)P_2$ to PI(4)P. Such dual phosphatase activity, 3- and 5-phosphatase activity, of VSP is highly conserved among orthologs, including sea squirt (11,12), zebrafish (13), chick (11), and human (14). The molecular basis underlying such broad substrate specificity in VSP despite structural similarity with PTEN still remains unclear. Substrate specificity of VSP seems intrinsic to the CCR, since chimera harboring VSD from sea squirt VSP (Ci-VSP) with the remaining region replaced by the human PTEN shows 3-phosphate specific enzyme activity similar to PTEN (15). Previous studies have identified some structural features of VSP that underlie substrate specificity distinct from PTEN. The motif in the active center, $Cx_5R$, the signature sequence common to cysteine-based phosphatases including protein tyrosine phosphatases and PTEN (6), is represented as CKGGKGR in VSP, where it is represented as CKAGKGR in PTEN; VSP has one different amino acid in the $Cx_5R$ motif from that of PTEN; alanine in PTEN is replaced by glycine in all VSP orthologs so far identified. G365A mutation in Ci-VSP remarkably reduced activity against $PI(4,5)P_2$, although it does not switch substrate specificity to a PTEN-like profile (12,16). Another clue was obtained by X-ray crystal structures of the cytoplasmic regions of Ci-VSP (12,17). They pointed critical roles of E411, which faces the substrate-binding pocket of Ci-VSP. Mutation of E411 in Ci-VSP altered phosphatase activity toward $PI(4,5)P_2$ (12,17). In PTEN, the site corresponding to E411 of Ci-VSP is on the loop called the TI loop, which was identified as one of the structural features of PTEN compared with protein tyrosine phosphatases (18). In the background of the chimera consisting of Ci-VSP's VSD and human PTEN's CCR (called Ci-VSPTEN), triple mutations of the two residues on this loop, T167 and I168, as well as A126 (corresponding to G365 of Ci-VSP) in the $Cx_5R$ motif resulted in converting 3-phosphate specific phosphatase activity into 5-phosphate-dominant phosphatase activity (19), indicating that both the $Cx_5R$ motif and TI loop are critical for determination of substrate specificity. On the other hand, reverse conversion of substrate specificity from VSP type to PTEN type based on site-directed mutagenesis has been unsuccessful so far.

Another important background behind the issue of substrate specificity of VSP is an apparent gap between in vitro phosphatase measurements and results of live cell measurements. The in vitro malachite green assay of the purified VSP's CCR polypeptide showed that $PI(3,4,5)P_3$ is a more dominant substrate than $PI(4,5)P_2$ for VSP (16,17), whereas measurements using live cell probes for PIPs indicate enzyme activity toward $PI(4,5)P_2$ is severalfold higher than for $PI(3,4,5)P_3$ (13,20). Comparison between results measured in live cells with in vitro biochemical assays is not straightforward, since the in vitro phosphatase assay was done with the protein that does not contain VSD. Grimm and Isacoff (21) suggested that $PI(3,4,5)P_3$ is more preferred substrate at the intermediate state of VSD activation, whereas activity toward $PI(3,4)P_2$ and $PI(4,5)P_2$ becomes more dominant when VSD is fully activated. Another study showed that higher expression of Ci-VSP in *Xenopus* oocyte induces dimerization and was accompanied by more evident voltage-dependent 3-phosphate activity toward $PI(3,4)P_2$ (20). A simulation of time courses of PIPs upon VSP activation in cells with different levels of expression recapitulated well the time courses obtained by experiments without the need of predicting distinct substrate preference between monomer and dimer (22).

In this study, we found by bioinformatics search that K364, a residue next to the active site cysteine of the $Cx_5R$ motif, is diversified in several mammalian VSP orthologs. Since the $Cx_5R$ motif of PTEN also has lysine at the same site, which is critical for its phosphatase activity (18,23), we attempted to ask whether these mammalian VSP orthologs have distinct enzyme activity than previously characterized VSP orthologs. Measurements of voltage-dependent change of $PI(4,5)P_2$ and $PI(3,4)P_2$ using Förster resonance energy transfer (FRET) probes in *Xenopus* oocyte showed that Ci-VSP mutants with amino acid change at K364 retained all of four subreactions: 5-phosphatase activity against $PI(4,5)P_2$ and $PI(3,4,5)P_3$ and 3-phosphatase activity against $PI(3,4)P_2$ and $PI(3,4,5)P_3$. Remarkably, K364M mutant showed increased activity both of 5-phosphatase against $PI(4,5)P_2$ and $PI(3,4,5)P_3$ and 3-phosphatase against $PI(3,4)P_2$. In vitro malachite green assay showed that the isolated CCR of K364M mutant has similar enzyme activities as the wild type (WT), suggesting tighter

**TABLE 1 Description of all Primers Used in this Research**

| For Mutagenesis | |
|---|---|
| K364 forward | aggggttatgacgaaacaaa |
| K364M reverse | cccgcccatacagtgaatcgc |
| K364I reverse | cccgcctatacagtgaatcgc |
| K364A reverse | cccgcctgcacagtgaatcgc |
| K364Q reverse | cccgccttgacagtgaatcgc |
| K364R reverse | cccgcctctacagtgaatcgc |
| C363S reverse | gcctttgctgtgaatcgctatcac |
| K364L forward | cactgtttaggcgggaagggaaga |
| K364L reverse | cccgcctaaacagtgaatcgctat |
| G214C forward | gccgattgtttggggagattggtt |
| G214C reverse | ccccaaacaatcggctcctgtttc |
| K303M forward | cactgcatgggaggaaagggtcgg |
| K303M reverse | cctcccatgcagtggatggcaata |
| Ci-Md-VSP forward | ctcgagatggagggattcgacggttc |
| Ci-Md-VSP reverse | ttaaaacagtagttccactgcgccggcg |
| Ci-Md-VSP joint forward | gtccaggtcaaatccatctttcctgtatcgacgctt |
| Ci-Md-VSP joint reverse | aagcgtcgatacaggaaagatggatttgacctggac |
| Ci-Md-VSP* forward | gaatgatatcagaaaacaagcgtcgatacaggaa |
| Ci-Md-VSP* reverse | tttctgatatcattcttctgcttgaagccttcatttg |
| **For Opossum cDNA Isolation** | |
| UTR5 Md-VSP forward | aagaaaagatgaaaaaacctc |
| UTR3 Md-VSP reverse | cccattcaataaacatttaat |
| Md-VSP NotI forward | ttttgcggccgcatggaagaaaaagagcacgg |
| Md-VSP Acc65I reverse | tttggtaccttaaaacagtagttccactg |

coupling between the CCR and VSD in K364M mutant than the WT. Further we exploited these findings to engineer a newer version of zebrafish VSP that can deplete $PI(4,5)P_2$ more efficiently in mammalian cells than previous versions.

## MATERIALS AND METHODS

### Plasmid and RNA synthesis

For *Ciona intestinalis* VSP (Ci-VSP), the previously described plasmid (24) was used. The F-TAPP or F-PLC plasmid were kindly provided by Dr. Ehud Isacoff (21). Bovine G-protein $\beta_1$ and $\gamma_1$ plasmids were kindly gifted by Dr. Toshihide Nukada. Mouse Kir3.2d (G-protein coupled inwardly rectifying $K^+$ channel 2d(GIRK2d)) plasmid was kindly provided by Dr. Yoshihisa Kurachi. The plasmid of the GFP-fused pleckstrin homology domain from PLC-$\delta$ subunit ($PH_{PLC\delta}$-GFP) was the same as we previously used (25). For electrophysiological experiments of Dr-VSP in HEK293T cell, K303M mutation was introduced in *e*VSP (CiDr-$VSP^{mChe}$ L223F in a customized pcDNA3.1(−) vector, L233F mutant of mCherry-fused chimeric Dr-VSP consisting of the N terminus of Ci-VSP and the main body of Dr-VSP (26)). EYFP-fused human Kv7.2 (KCNQ2) and Kv7.3 (KCNQ3) were kindly provided by Dr. Bertil Hille.

Opossum DNA encoding VSP was synthesized (Thermo Fisher Scientific, USA) and amplified based on the sequence registered in Genbank (XM_007495378.2) (Thermo Fisher Scientific). The synthesized DNA fragments were amplified by using primers (Table 1) and subcloned into NotI and Acc65I sites of pSD64TF (kindly gifted from Dr. Terry Snutch). The full-length cDNA was also subcloned through RT-PCR using testis cDNA pool (kindly provided by Dr. Hiroshi Kiyonari, RIKEN Center for Biosystems Dynamics Research). cDNA sequence obtained by this subcloning was identical to that described in Genbak: XM_007495378.2. Ci-Md-VSP chimeric DNA was generated using Ci-VSP and Md-VSP as templates using PCR primers (Table 1) and subcloned into pSD64TF. To obtain another form of chimera harboring a closer amino acid sequence in the VSD-PD linker region to Md-VSP (designated as Ci-Md-VSP*, Fig. S4), double mutation (T247M/Q250E) was introduced into Ci-Md-VSP by PCR. DNA sequence of all constructs were confirmed through Sanger sequencing.

cRNAs were synthesized using mMESSAGE mMACHINE SP6 or T7 kit (Thermo Fisher Scientific). Bovine G-protein $\beta_1$, $\gamma_1$, $PH_{PLC\delta}$-GFP, and Ci-VSP plasmids were linearized by XbaI. Mouse-Kir3.2d plasmid was linearized by SphI. F-TAPP and F-PLC plasmids were linearized by NheI. All point mutations of Ci-VSP (C363S, G214C, K364I, K364A, K364Q, K364R, K364L, K364M) were introduced using a forward primer upstream of mutagenesis site and a reverse primer carrying the mutant site (Table 1). PCR was performed using PrimeSTAR Max (Takara Bio, Japan). PCR primers are listed on Table 1. Mutations introduced by mutagenesis were confirmed through Sanger sequencing.

For malachite green assay, the CCR of Ci-VSP (amino acids 240–576) was inserted into NdeI and SalI sites of pET-21b (+) or NcoI and SalI of pET-28b (+). All point mutations (C363S, K364L, K364R, K364M) were introduced using a forward primer upstream of the mutagenesis site and a reverse primer carrying the mutant site.

### Database search

The amino acid sequences of VSP orthologs were searched in the UniProtKB, and we followed their taxonomy tree to find the sequences (https://www.uniprot.org/uniprot/?query=tpte2&fil=&sort=score#orgViewBy). The phylogenetic trees of VSP orthologs were constructed by maximum likelihood test with MEGA 11 (27) and drawn on iTOL v6 (https://itol.embl.de/).

### *Xenopus* oocyte expression

Oocytes were collected from *Xenopus laevis* anesthetized in distilled water containing 0.2% ethyl 3-aminobenzoate methanesulfonate salt (Sigma-Aldrich, USA or Tokyo Chemical Industry, Japan). Experiments were performed according to the guidelines of the Animal Research Committees of the Graduate School of Medicine of Osaka University. The oocytes were defolliculated using type I collagenase (Sigma-Aldrich) or Collagenase P (Roche, Switzerland) and injected with cRNA as described below. The synthesized cRNA was diluted to the following concentrations: Ci-VSP (100 ng/μL), Ci-Md-VSP (100 ng/μL), F-PLC (100 ng/μL), F-TAPP (100 ng/μL), GIRK2d with bovine G-protein $\beta_1$ and $\gamma_1$ (150 ng/μL), and Ci-VSP G214C mutants (80 ng/μL). About 50 nL of cRNA was injected into defolliculated oocytes, and oocytes were incubated in ND96 (96 mM NaCl, 2 mM KCl, 1.8 mM $CaCl_2$, 1 mM $MgCl_2$, 5 mM HEPES, pH 7.5 with NaOH) supplemented with 0.1 mg/mL gentamycin (Nacalai Tesque, Japan) and 5 mM sodium pyruvate for 2 days (F-PLC, GIRK2d, and Ci-VSP G214C mutants) or 3 days (F-TAPP) at 18°C after injection.

### Voltage clamp fluorometry recording with FRET probes (F-PLC and F-TAPP)

The microscope IX71 (Olympus, Japan) was used with a 20 × 0.75 numerical aperture (NA) objective lens and an arc lamp with mercury burner, fitted with an excitation filter of 438 nm/24 nm (Semrock, USA) with a dichroic (DM458, Semrock) and an emission filter of 470 nm/100 nm (Semrock) for the cyan fluorescent protein (CFP )channel and 525 nm/39 nm (Semrock) for the YFP channel with a dichroic (DM510, Semrock). The emitted light was detected by two photomultiplier tubes (PMTs) (H10722-20; Hamamatsu Photonics, Japan). Two-electrode voltage clamp (TEVC) recording was done using the amplifier, Oocyte Clamp OC-725C (Warner Instruments, USA) at room temperature (22°C–24°C). Before recording of FRET signal after voltage clamping of oocyte to a holding potential of −60 mV, voltage for PMT was adjusted so that PMT gain both of CFP channel and YFP channel became similar at around 4.0 V (Fig. S2). Output signals were digitized using Digidata 1440A (Molecular Devices,

USA) run by the software pClamp 10.3 (Molecular Devices) with 10-kHz sampling rate on Windows PC. After digitization, data were filtered using Gaussian digital filter at cutoff frequency of 10–50 Hz on Clampfit software (Molecular Devices). The bath solution was ND96, the glass electrodes were filled with 3 M KCl, and the resistances ranged from 0.2 to 1.0 MΩ. The holding potential was −60 mV. Before starting FRET measurement, membrane potential of cells was set to −60 mV for more than 1 min. We assume that enzyme activity of Ci-VSP is silent at −60 mV, but we cannot completely exclude a possibility that Ci-VSP has some voltage-independent latent enzyme activity with down state of voltage sensor. A depolarizing pulse (0–150 mV) was applied for 5 s. Since PMT gain was not able to be adjusted completely between the YFP channel and CFP channel in some cases, YFP/CFP ratio before running a step protocol for stimulation was not exactly equal to 1.0. In data analysis, the signal of YFP/CFP before applying the test pulse was defined as the baseline YFP/CFP signal, and $\Delta$FRET was measured as the proportion of deviation from the baseline against the baseline YFP/CFP signal. In this study, data were analyzed based on the assumption that resting levels of phosphoinositides are similar among cells.

To estimate cell surface expression level of Ci-VSP and its mutants (Figs. S6 *C* and S7 *C*), sensing currents were also measured from the same cells used for FRET measurement, and the maximum charges of off-sensing current ($Q_{OFF}$) were calculated by integration of the $Q_{OFF}$ that extends 150 ms from the end of the depolarizing step. Sensing current was evoked by depolarizing steps from the holding potential of −60 to 160 mV. Leak subtraction was performed using a P/8 protocol. The same bath solution for FRET measurement was used.

To compare the charge-voltage relationship among mutants (Fig. S5), sensing current was measured from oocytes expressing Ci-VSP alone using sodium-free bath solution (105 mM n-methylglucamine (NMDG), 2 mM $MgCl_2$, 0.1 mM EGTA, 10 mM HEPES, pH 7.5 with methanosulfonate). Sensing currents were evoked by depolarizing steps from the holding potential of −60 mV to 200 mV in 10-mV increments. Leak subtraction was performed using a P/-4 protocol. All recordings were done at room temperature (22°C–24°C).

## Voltage clamp fluorometry recording with $PH_{PLC\delta}$-GFP

To examine subreaction from $PI(3,4,5)P_3$ to $PI(4,5)P_2$ by WT and mutant Ci-VSPs, we utilized $PH_{PLC\delta}$-GFP (11,25) as the probe for $PI(4,5)P_2$ instead of F-PLC, since the magnitude of increase of F-PLC signal due to subreaction from $PI(3,4,5)P_3$ to $PI(4,5)P_2$ is minute or often not detected. Since $PI(3,4,5)P_3$ level is very low in *Xenopus* oocytes, oocytes expressing both Ci-VSP and $PH_{PLC\delta}$-GFP were preincubated in ND96 with 17 μM insulin (FUJIFILM Wako Pure Chemical Corporation, Japan) for 10 min at room temperature to increase resting level of $PI(3,4,5)P_3$. Except for excitation and emission filters (BP460-480HQ (Olympus) and BA495-540HQ (Olympus), respectively), the same setup for FRET measurement was used. The emitted fluorescence was detected by single PMT. Oocytes were depolarized to 50 mV from the holding potential of −60 mV for 10 s in ND96. All recordings were done at room temperature (22°C–24°C).

## Voltage clamp fluorometry recording of voltage sensor motion using tetramethylrhodamine maleimide conjugated on G214C in *Xenopus* oocyte

Tetramethylrhodamine maleimide (TMRM) was labeled on G214C on the S3-S4 linker of Ci-VSP after the previous papers (28,29). The microscope, digitizer, amplifier, and software were the same as were used for FRET probe recording. BP535-555, BP570-625, and DM565 (Olympus) were used for the excitation filter, emission filter, and dichroic mirror, respectively. Fluorescence was measured using single PMT.

Oocytes expressing G214C mutants were incubated with 10 μM TMRM (Invitrogen, USA) for 1 h at 18°C in ND96. Oocytes were then washed twice with ND96 and kept in the dark until recording.

The bath solution was ND96. A depolarizing pulse was stepped to the level between −60 and 200 mV in 10-mV increments for 500 ms. The set of pulses was repeated six or eight times, and acquired fluorescence data were averaged. All recordings were done at room temperature (22°C–24°C).

## GIRK2 current recording from *Xenopus* oocyte

To evaluate the phosphatase activity of Ci-VSP, GIRK2d with bovine G-protein $\beta_1$ and $\gamma_1$ was coexpressed with WT or mutant Ci-VSP. TEVC recordings were done using an OC-725C amplifier through an AD/DA converter (Digidata 1440A or InstruTECH LIH 8 + 8: HEKA Elektronik) running under pClamp or PatchMaster software (HEKA Elektronik), respectively at room temperature (22°C–24°C). Output signals were digitized at 10 kHz. The bath solution was ND96, the glass electrodes were filled with 3 M KCl, and the resistances ranged from 0.2–1.0 MΩ. The holding potential was −60 mV. Decay rate was measured by fitting time course of magnitude of GIRK2 current upon repeated VSP stimulations with single exponential function.

## Electrophysiological studies of Dr-VSP K303M mutant in HEK293T cell

HEK293T cells were cultured in DMEM (FUJIFILM Wako Pure Chemical Corporation) supplemented with 10% fetal bovine serum (Biowest, France) and penicillin/streptomycin (10 μg/mL, Nacalai Tesque) at 37°C in an incubator with 5% $CO_2$. To measure the phosphatase activities of VSP, cDNA of VSP was cotransfected with that of KCNQ2 and KCNQ3 using Polyethylenimine (PEI) Max reagent (Polysciences, USA). Between 5 and 6 h after transfection, the medium was refreshed and then cells were incubated for 10–15 h. Transfected cells were reseeded into poly-L-lysine (Sigma-Aldrich)-coated dishes. Electrophysiological recordings were performed 2–10 h after reseeding.

Macroscopic $K^+$ currents were recorded in the whole-cell patch configuration using an Axopatch-200B amplifier (Molecular Devices) through an AD/DA converter (Digidata 1322A: Molecular Devices) running under pClamp software at room temperature (22°C–24°C). Current traces were filtered at 5 kHz using a four-pole Bessel filter and sampled at 10 kHz. Patch pipettes were pulled from borosilicate glass (Drummond Scientific Company, USA), and their resistances were 3–10 MΩ after filling with the pipette solution containing 100 mM KCl, 3 mM $MgCl_2$, 1 mM EGTA, 20 mM HEPES, and 2 mM ATP-$Na_2$ (pH 7.2 and 300 mOsm adjusted with KOH and glucose, respectively). The bath solution contained 10 mM KCl, 90 mM NaCl, 1 mM $MgCl_2$, 1 mM $CaCl_2$, and 20 mM HEPES (pH 7.2 and 300 mOsm adjusted with NaOH and glucose, respectively). The holding potential was set to −60 mV. The pulse protocol used to estimate the phosphatase activity of VSP consists of a 300-ms test step pulse from the holding potential to 0 mV and a 300-ms depolarizing pulse to 0, 25, 50, or 75 mV. This was repeated 11 times without any intervals.

To evaluate the charge-voltage (*Q-V*) relationship, sensing current was measured from cells expressing VSP alone with symmetric pipette and bath solutions containing 75 mM NMDG, 3 mM $MgCl_2$, 1 mM EGTA, and 180 mM HEPES, adjusted to pH 7.0 and 300 mOsm with methanesulfonate and glucose, respectively. Pipette resistance was 7–15 MΩ. Sensing currents were evoked by depolarizing steps from the holding potential of −60 to 200 mV in 10-mV increments. Leak subtraction was performed using a P/-8 protocol.

## Synthesis of tagged protein and purification

All CCR of Ci-VSP (240–576) were fused with an N-terminal GFP-8His-myc-8His and TEV protease cleavage site. The plasmid was transformed into BL21-CodonPlus(DE3)-RIPL Competent Cells (Agilent) and cells were

grown at 37°C in Luria-Bertani (LB) medium until an optical density 660 ($OD_{660}$) of 0.6–0.8 was reached. Protein expression was induced by 0.3 mM IPTG and cultures were incubated at 20°C. Cells were harvested by centrifugation at 5000 × *g* for 10 min at 20°C, frozen using liquid nitrogen, and kept at −30°C until use. Cell were thawed and lysed by sonication in sonication buffer (20 mM Tris pH 7.5, 300 mM NaCl, 2 mM dithiothreitol (DTT)). Lysate was centrifuged at 40,000 × *g* for 30 min at 4°C, and supernatant was applied to Ni-NTA agarose (Qiagen). Ni-NTA beads were washed with wash buffer (20 mM Tris pH 7.5, 300 mM NaCl, 25 mM imidazole pH 7.5, 2 mM DTT), and protein was eluted with elution buffer (20 mM Tris pH 7.5, 150 mM NaCl, 250 mM imidazole pH 7.5, 2 mM DTT). Tobacco Etch Virus (TEV) protease was added to the eluted protein to digest the tag. To remove the tag, the protein was applied to Ni-NTA and flow-through was collected. The cleaved protein was applied to HiTrap SP HP (Cytiva) and eluted in a NaCl gradient. Fractions containing Ci-VSP were collected, concentrated, and applied onto Superdex 200 Increase (Cytiva) in a gel filtration buffer (20 mM Tris pH 7.5, 150 mM NaCl, 2 mM DTT). The purified protein was pooled and concentrated to 1–2 mg/mL, flash frozen using liquid nitrogen, and stored at −80°C.

### Malachite green assay

The malachite green assay was performed according to previous reports (11,16,17,29). D-myo-inositol 1-[(2R)-2,3-bis[(1-oxohexadecyl)oxy]propyl hydrogen phosphate][di-$C_{16}$-PI(3,4,5)$P_3$], 1-(1,2R-dihexadecanoylphosphatidyl)inositol-3,4-bisphosphate [di-$C_{16}$-PI (3,4)$P_2$], 1-(1,2-dihexadecanoylphosphatidyl)inositol-4,5-bisphosphate [di-$C_{16}$-PI(4,5)$P_2$), 1-(1,2R-dihexadecanoylphosphatidyl)inositol-3,5-bisphosphate [di-$C_{16}$-PI(3,5)$P_2$] (Cayman, USA), and 1-palmitoyl- 2-oleoyl- sn-glycero-3- phosphatidylserine (POPS; Avanti Polar Lipids, USA) were used for the assay. The 100 nmol of PIPs and 10 nmol of POPS were dried together under reduced pressure and resuspended in 9 μL of buffer solution (100 mM Tris-HCl (pH 8.0), 10 mM DTT, 0.04% (v/v) NP-40) using a sonicator bath. The reaction was started by adding 1 μL of CCR of Ci-VSP or mutant (1 mg of protein) at 23°C. After 1 h, the reaction was stopped by adding 15 μL of 100 mM N-ethylmaleimide (NEM) and the mixture was centrifuged to remove aggregates. Then 20 μL of the supernatant was mixed with 100 μL of BIOMOL Green reagent (Enzo Life Sciences, USA) and incubated for 40 min at room temperature. Absorbance at 620 nm was measured with a microplate reader (MultiScan FC: Thermo Fisher Scientific, USA).

### Data analysis

Data are presented as mean ± SE. Single exponential fitting was done with Python v.3.8 (https://www.python.org/), numpy v.1.21.2 (https://numpy.org/), Matplotlib v.3.4.3 (https://matplotlib.org/), and SciPy 1.7.1 (https://www.scipy.org/). Double exponential fitting was done using Clampfit software. Sigmoidal curve fitting was done using Igor Pro 6.0 (WaveMetrics, USA). One-way ANOVA followed by Dunnett's multiple comparisons test was performed using GraphPad Prism version 9.0.0 for Windows (GraphPad Software, USA). Data analysis was performed using Microsoft Excel and Igor Pro.

## RESULTS

### Phylogenetic diversity of enzyme active site of VSP between some marsupials and other animals

The amino acid sequences of VSP orthologs were extensively searched from online databases based on the full-length coding sequence of sea squirt VSP (*Ciona intestinalis* VSP; Ci-VSP). We found some VSP orthologs from mammalian species showed amino acid diversity in the highly conserved $Cx_5R$ motif of enzyme active center (Figs. 1 and S1). At the site corresponding to K364, next to the active site cysteine in the $Cx_5R$ motif of Ci-VSP, predicted polypeptide sequences of VSP orthologs from certain members of the Marsupialia (koala, Tasmanian devil, and common wombat) showed methionine and that of short-tailed opossum has leucine. Such amino acid change is not only found in orthologs of Marsupialia but also in those of other mammals; an ortholog of prairie deer mouse has methionine, and that of northern white-cheeked gibbon has asparagine at the site. Amino acid diversity at this site was not found in the VSP orthologs from non-mammal vertebrates and invertebrates based on the online database in the autumn of 2022.

### Ci-Md-VSP, a chimeric VSP between orthologs of *C. intestinalis-Monodelphis domestica*, shows voltage-dependent PIPs phosphatase activities

PTEN has highly conserved lysine, K125, at the site corresponding to K364 of Ci-VSP (Fig. 1 *A*), and mutation of this site in human PTEN results in remarkable reduction of 3-phosphatase activity (18,23). Some human cancer patients have amino acid mutation at this site (COSMIC database). On the other hand, this lysine in the $Cx_5R$ motif is also conserved in PI(5)P phosphatase, called PLIP (30). Therefore, we wondered if mammalian VSP orthologs containing non-K residue at this site might exhibit substrate specificity distinct from that in previously characterized VSPs, sea squirt VSP (Ci-VSP), zebrafish VSP (Dr-VSP), mouse VSP (Mm-VSP), and human VSP (Hs-VSP) (11,14,31,32). The full-length cDNA sequence of opossum VSP (*Monodelphis domestica* (Md)-VSP) was obtained by RT-PCR from opossum testis cDNA pools. Predicted amino acid sequence was identical to that registered on Genbank (XM_007495378.2).

The coding sequence of Md-VSP was subcloned into in vitro transcription plasmid vector, and cRNA encoding Md-VSP was expressed in *Xenopus* oocyte. We examined voltage-sensing function and voltage-sensitive phosphatase activity as previously established (24,25), respectively. We failed to see any trace of sensing currents (also called gating currents) from oocytes expressing Md-VSP, which represents motion of voltage sensor, and voltage-dependent change of activity of GIRK2 channel coexpressed with Md-VSP. These are probably due to insufficient cell surface targeting of Md-VSP as previously reported in other mammalian VSP orthologs (6,14,32,33). In fact, when Md-VSP was expressed in HEK293T cells, we found that the protein was not targeted to cell surface as detected by immunofluorescence analysis using antibody to FLAG-tag sequence fused to Md-VSP (data not shown).

Then, we made a chimera by joining the transmembrane area of Ci-VSP with CCR of Md-VSP at the VSD-PD linker region (Fig. 2 *B*). The chimeric construct (designated as

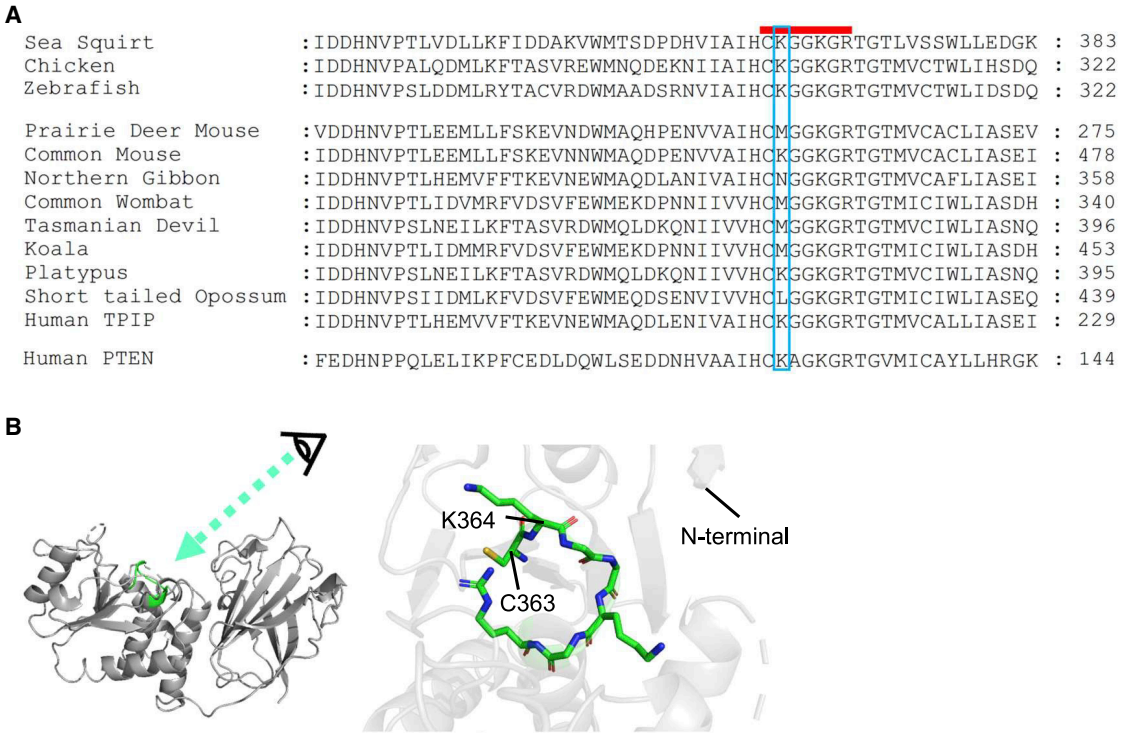


FIGURE 1 Structure of sea squirt VSP (Ci-VSP) PD and amino acid alignment of the enzyme active center region containing the $Cx_5R$ motif in nine mammalian VSPs with Ci-VSP, zebrafish VSP (Dr-VSP), chick VSP, and human PTEN. (*A*) Amino acid sequence containing the enzyme active center region of mammalian VSP orthologs aligned with that of Ci-VSP and human PTEN. Red thick bar indicates the conserved $Cx_5R$ motif in the enzyme active center of the PD. The blue box highlights the 364th residue of Ci-VSP and corresponding site in other orthologs and PTEN. The VSP sequences of sea squirt (*Ciona intestinalis*, Genbank: NM_001033826.1), human (TPIP, Genbank: NP_001135440.1), chicken (*Gallus gallus*, UniProtKB: E1BUX1_CHICK), common mouse (*Mus musculus*, Genbank: NP_954866.2), northern white-cheeked gibbon (Genbank: XM_030813293.1), prairie deer mouse (*Peromyscus maniculatus bairdii*, Genbank: XM_016001573.1), koala (*Phascolarctos cinereus*, Genbank: XM_020970026.1), common wombat (*Vombatus ursinus*, Genbank: XP_027712713.1), Tasmanian devil (*Sarcophilus harrisii*, Genbank: XM_031961971), opossum (*Monodelphis domestica*, Genbank: XM_007495378.2), platypus (*Ornithorhynchus anatinus*, UniProtKB: F6X178_ORNAN), and human PTEN (UniProtKB: P60484 (PTEN_HUMAN)) were aligned using ClustalX2.1 (European Bioinformatic Institute). Amino acid numbers at the last position shown in the alignments are shown for each ortholog and human PTEN. (*B*) Left: the CCR of Ci-VSP (PDB: 3AWF) with the $Cx_5R$ motif, which corresponds to the red thick bar in (*A*). Upper side faces cell membrane. The PD (the left half of the structure) mainly consists of $\alpha$ helices, whereas the C2 domain (the right half) mainly consists of $\beta$ sheets. The enzyme active center containing the $Cx_5R$ motif (*green*) resides in PD. Right: the enlarged structure viewed from the direction of "Eye" on the left panel.

Ci-Md-VSP) consisted of the regions Ci-VSP (1–257) and Md-VSP (314–625).Voltage-dependent phosphatase activity against $PI(4,5)P_2$ was examined by performing experiments of voltage clamp fluorometry (VCF) from *Xenopus* oocytes coexpressing Ci-Md-VSP with fluorescent $PI(4,5)P_2$-specific probe, F-PLC(21). F-PLC is a FRET probe where CFP and YFP sandwich PLC-δ pleckstrin homology (PH) domain, which selectively binds to $PI(4,5)P_2$. When $PI(4,5)P_2$ binds to the PH domain, CFP and YFP are brought in close proximity to emit yellow fluorescent light after excitation with blue light and the ratio of YFP signal versus CFP signal (YFP/CFP) reflects abundance of $PI(4,5)P_2$ levels (Fig. 2 *C*) (21). Voltage-evoked decrease of FRET signal was observed at 25 mV or higher voltage representing decrease of $PI(4,5)P_2$ level caused by Ci-Md-VSP's enzyme activity (Fig. 2 *D* left column, and *E*). The extent of decay becomes more remarkable as the voltage is more positive (Fig. 2 *D* left column, and *E*). We also measured $PI(4,5)P_2$ enzyme activity of Ci-Md-VSP using GIRK2 channel (23,27,30,31). GIRK2 channel was coexpressed with G-protein $\beta$ and $\gamma$ subunits and VSPs, and decay rate of Kir current upon $PI(4,5)P_2$ decrease with repeated conditioning membrane depolarizations, which activate VSP enzyme activity, was measured. Decay rate represents the extent of enzyme activity. Decay of GIRK2 currents becomes sharper as the voltage is increased (Fig. 2 *F* and *G*), consistent with the results of F-PLC.

Voltage-dependent phosphatase activity of Ci-Md-VSP against $PI(3,4,5)P_3$ and $PI(3,4)P_2$ was also examined by using another FRET probe, F-TAPP, which is based on a similar design to F-PLC but to sense $PI(3,4)P_2$ (21). In oocytes expressing Ci-VSP as positive control, a clear depolarization-evoked biphasic pattern of F-TAPP's FRET signal was observed, representing early production of $PI(3,4)P_2$ by dephosphorylation of $PI(3,4,5)P_3$ and later a 3-phosphatatase reaction against $PI(3,4)P_2$ (Fig. 2 *D* right column, and Fig. S2). There was little change of F-TAPP signal in oocytes that only express F-TAPP without

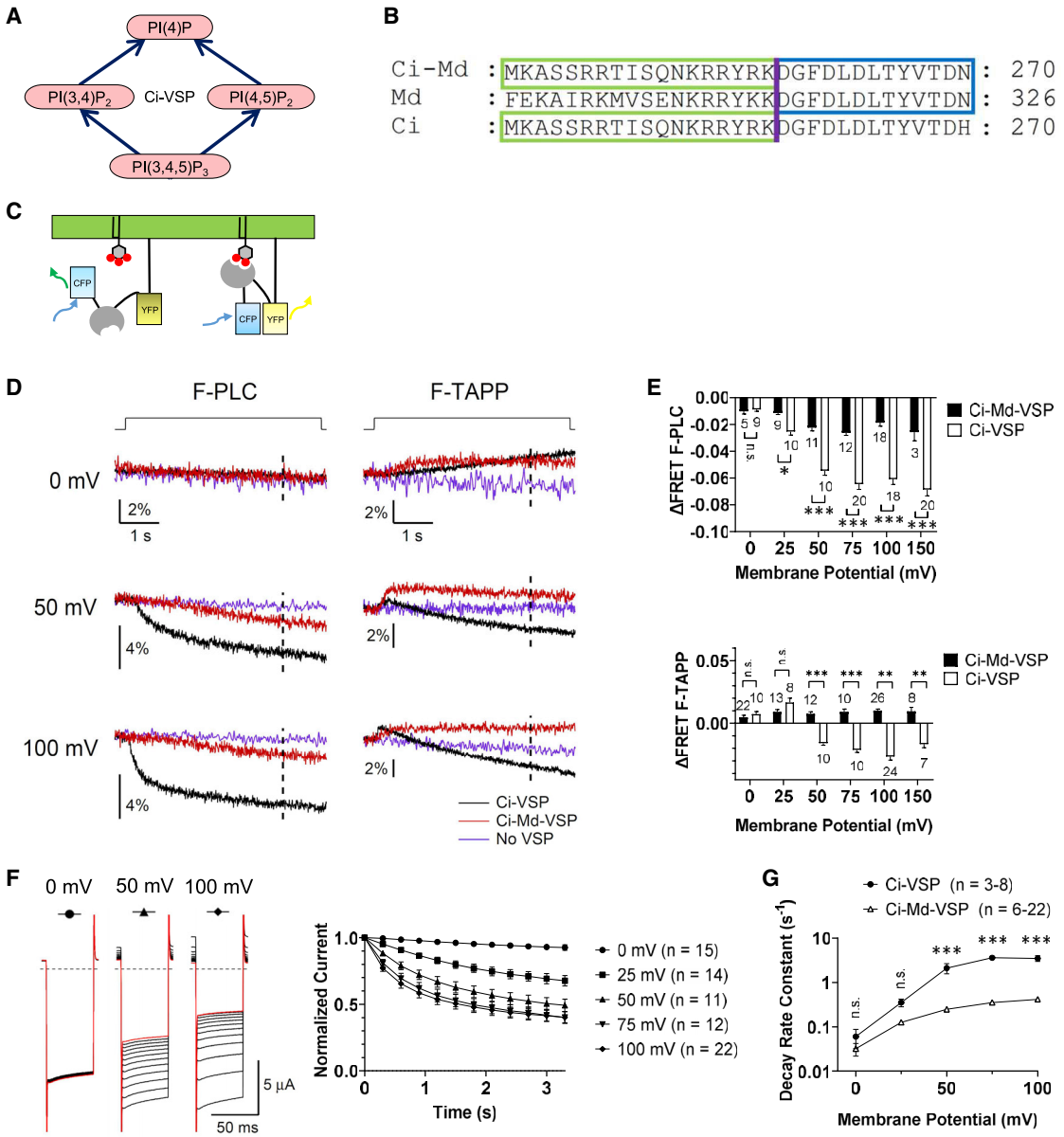


FIGURE 2 Characterization of voltage-dependent phosphoinositide phosphatase activity of the sea squirt-opossum VSP chimera, Ci-Md-VSP in *Xenopus* oocyte. (*A*) Four subreactions of PIPs dephosphorylation mediated by VSP. (*B*) Amino acid sequences around the junction region of chimeric construction between Ci-VSP and Md-VSP. Ci-Md, Md, and Ci denote the Ci-Md-VSP, Md-VSP, and Ci-VSP, respectively. (*C*) A scheme of FRET probe, F-PLC or F-TAPP, for sensing $PI(4,5)P_2$ or $PI(3,4)P_2$, respectively, consisting of the two fluorescent proteins (*box*) sandwiching the PH domain (*gray*) selective to each species of PIP. (*D*) Representative traces for YFP/CFP ratio of F-PLC (*left*) and F-TAPP (*right*) with Ci-VSP (*black*), Ci-Md-VSP (*red*), or without VSP (no VSP, *purple*) at indicated voltage. Traces are normalized to baseline level of fluorescence before depolarization. Depolarizing step shown at top of traces was applied from a holding potential of −60 mV to indicated value for 5 s. Dotted line in each trace indicates the time point (at 4 s after the beginning of depolarization) for calculating ΔFRET. (*E*) Graph showing ΔFRET for F-PLC (*top*) and F-TAPP (*bottom*) at six voltages for Ci-Md-VSP and Ci-VSP. The number of recordings is shown within the graph. *p < 0.05; **p < 0.01; ***p < 0.001; n.s., statistically not significant, two-tailed unpaired *t*-test. Data are presented as mean ± SE. (*F*) *Left*: representative GIRK2 traces in oocytes expressing Ci-Md-VSP. GIRK2 currents were evoked by hyperpolarizing steps from the holding potential of −60 to −120 mV and then oocytes were depolarized to 0, 50, or 100 mV for 300 ms. This was repeated 12 times, and all GIRK2 traces are superimposed (see also Fig. S3). The 12th traces are shown in red. Black dotted lines indicate zero current level. *Right*: time course of GIRK2 current upon voltage-evoked VSP activities with five levels of conditioning depolarization. The current amplitudes were normalized to that in the first trace. Data are presented as mean ± SE. (*G*) Decay rate constant of the normalized GIRK2 current ($s^{-1}$) at different potentials. GIRK2 was coexpressed with Ci-VSP or Ci-Md-VSP. *p < 0.05; **p < 0.01; ***p < 0.001; n.s., statistically not significant, two-tailed unpaired *t*-test. Data are presented as mean ± SE.

Ci-VSP, as previously reported (21) (shown as purple in Fig. 2 *D*). In contrast with Ci-VSP (black traces in Fig. 2 *D*), decline of F-TAPP signal subsequent to early rise was less remarkable in oocytes expressing Ci-Md-VSP. This may suggest that, in Ci-Md-VSP, the activity of 5-phosphate dephosphorylation of $PI(3,4,5)P_3$ to $PI(3,4)P_2$

was robust, whereas 3-phosphate dephosphorylation of $PI(3,4)P_2$ to PI(4)P was weak. However, it is possible that weaker activity toward $PI(3,4)P_2$ of Ci-Md-VSP than Ci-VSP is due to low expression level of Ci-Md-VSP protein since temporal profile of F-TAPP signal is known to depend on expression level of VSP (20,22). We performed measurements of maximum charges of off-sensing currents in TEVC recordings, which provide a reliable indicator for cell surface expression level of VSP (25). However, Ci-Md-VSP showed only low magnitude of sensing current and was not well separated from endogenous currents, which made it difficult to evaluate cell surface expression level (data not shown). As an alternative possibility of weak voltage-dependent enzyme activity of Ci-Md-VSP, coupling between VSD and enzyme is not sufficient due to structural mismatch between PD and VSD-PD linker in the chimeric protein, since a previous report suggested that matching between PD and VSD-PD linker is critical for efficient voltage-dependent phosphatase activity (15). Ci-VSP and Md-VSP show amino acid sequences diversity in the VSD-PD linker. Therefore, the VSD-PD linker was made more similar to that of Md-VSP. Double mutation of T247M/Q250E was introduced into Ci-Md-VSP (designated as Ci-Md-VSP*; Fig. S4) and voltage-dependent phosphatase activity was measured using GIRK2 currents as the reporter. However, it only showed slight improvement of voltage-dependent enzyme activity. We also tested another version of Ci-Md-VSP by more extensively altering amino acids at the proximal VSD-PD linker region. However, we failed to record its phosphatase activity in oocytes because oocytes expressing this chimeric protein died, probably of toxicity by this protein.

## Comparison of voltage sensor motion among WT and K364 mutants

Since cell surface expression of Ci-Md-VSP was not robust in *Xenopus* oocyte, we decided to explore implications of amino acid diversity of lysine in $Cx_5R$ by performing site-directed mutagenesis analysis using Ci-VSP as the model molecule. Corresponding to amino acid change to leucine in the VSP ortholog of short-tailed opossum, K was changed to L (Ci-VSP K364L). K364 of Ci-VSP was changed to M (Ci-VSP K364M), corresponding to the amino acid in the orthologs from prairie deer mouse, Tasmanian devil, common wombat, and koala. To obtain mechanistic insights, four other amino acids, A, I, R, and Q, were also introduced to this site.

To verify their cell surface expression, sensing currents of K364 mutants were recorded by TEVC from *Xenopus* oocytes and compared with those of the WT (Fig. S5). A plot of $Q_{OFF}$, moving charges of off-sensing currents, over a range of membrane potential showed that mutants had similar voltage dependence to the WT (Fig. S5 *B*, right column) except that K364A showed minor rightward shift of the $Q_{OFF}$-$V$ curve (Fig. S5 *B*). Decay kinetics of off-sensing currents (Fig. S5 *C*) of all mutants became slower with increase of depolarizing level, which is characteristic of WT Ci-VSP, as previously reported (24).

We then performed VCF using TMRM, an environment-sensitive fluorescent reporter. It has been reported that TMRM is attached to a cysteine near the external end of the S4 helix and changes its light intensity as a function of their hydrophilic/hydrophobic environment (21,28). To label TMRM, a cysteine was introduced at position G214 following the previous study (28). For clarity, the G214C mutants will be referred to simply as WT or K364 mutant. Robust fluorescence signal was obtained from oocytes expressing all mutants (Fig. 3 *A*). Compared with WT, a slight shift of the fluorescence-voltage (*F-V*) relationship as evidenced by comparison of the values of $V_{Half}$, the voltage that gives half of the maximum fluorescence change, was found in K364L and K364Q ($p < 0.05$ and $p < 0.01$, respectively) (Fig. 3 *B* and *C*). K364L had steeper slope than other mutants and WT representing saturation of signal at lower voltage than other constructs. Some differences in kinetics among mutants were observed (Fig. 3 *A* and *D*). K364M showed the slowest speed upon both depolarization and repolarization. K364L showed slightly slower recovery upon repolarization than WT (trace at 100 mV of Fig. 3 *A*).

## Phosphatase activity against $PI(4,5)P_2$ in Ci-VSP with mutation of K364

To determine voltage-dependent enzyme activities of K364 mutants against $PI(4,5)P_2$, VCF was performed from *Xenopus* oocytes coexpressing a $PI(4,5)P_2$-sensing fluorescent protein (F-PLC) with VSP. FRET signal of F-PLC fluorescence as YFP/CFP ratio was measured by the TEVC recording (Figs. 4 and S6). Cell surface expression of Ci-VSP mutant from the individual same cell for VCF recording was verified by measuring sensing currents followed by analysis of maximum charge values of off-sensing currents derived from the voltage sensor motion of the Ci-VSP mutants ($Q_{OFF}$). Values of $Q_{OFF}$ showed that K364I/R/Q/M were expressed as robust as the WT (Fig. S6 *C*), whereas $Q_{OFF}$ of K364A and K364L was slightly smaller than that of the WT. Representative traces of FRET signal are shown in Fig. 4 *A* and S6 *A*. All mutants showed voltage-dependent decrease of F-PLC FRET signal upon membrane depolarization. The extent of voltage-dependent change of F-PLC FRET signal ($\Delta$FRET) was quantified by measuring the shift from the baseline at different voltage levels (Figs. 4 *B*, *C*, and S6). At 100 mV (Fig. 4 *B*, bottom) and 150 mV (Fig. S6 *B*, bottom), all mutants showed similar saturated level of $\Delta$FRET to that of WT. At voltages 0, 25, 50, and 75 mV, the size of $\Delta$FRET was significantly smaller in K364 A/R/Q than WT, whereas K364M showed larger size of $\Delta$FRET. However, kinetics of F-PLC signal became more rapid at 100 mV than at 50 mV, whereas $\Delta$FRET level

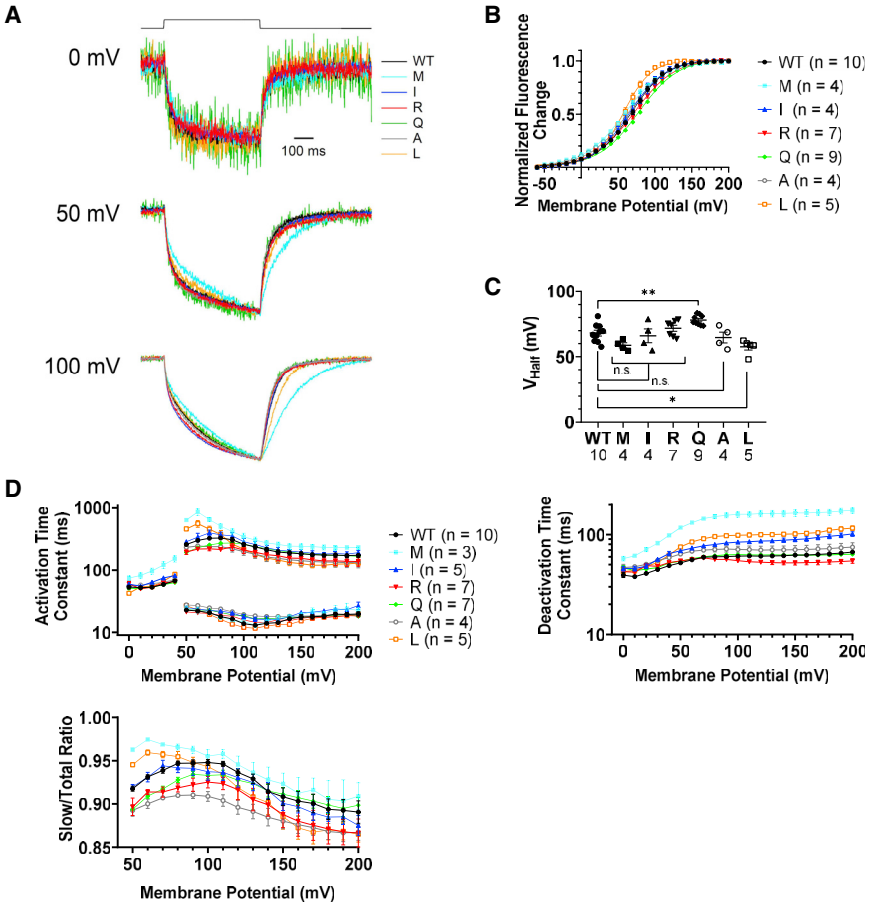


FIGURE 3 Characterization of VSD motions of Ci-VSP K364 mutants by VCF of TMRM labeled on S3-S4 linker. (*A*) Superimposed representative normalized VCF data of the WT and six K364 Ci-VSP mutants (shown in different colors) upon a step to 0, 50, and 100 mV. Traces are normalized by the fluorescence level at the baseline and the size of maximum change of fluorescence across mutants and the WT. (*B*) F-V curves for WT and K364 mutants. Data are presented as mean ± SE. Curves are Boltzmann fits. (*C*) Voltage that gives half of the maximum fluorescence change ($V_{Half}$), acquired by fitting the F-V curve with the equation $(FL(V)/FL_{MAX} = 1/[1 + \exp\{-ZF(V-V_{Half})/RT\}]$, where $F$ is Faraday constant, $R$ is the gas constant, $T$ is the absolute temperature, $Z$ is the effective valency, V is voltage, and $FL_{MAX}$ is the maximum fluorescence change. The number of recordings is shown at the bottom of the graph. Data are presented as mean ± SE. *p < 0.05; **p < 0.01; n.s., statistically not significant, one-way ANOVA followed by Dunnett's test. (*D*) Left: the time constant by fitting the activation phase of TMRM fluorescence with a single exponential function from 0 to 40 mV, and with a double exponential function more than 50 mV of K364 mutants and the WT (*top*). The proportion of the slow component is shown at the bottom. *Right*: the time constant of the deactivation phase fitted with a single exponential function. Data are presented as mean ± SE.

was similar between the two voltages both in WT and K364M (Fig. 4 *A*). This suggests that phosphatase activity against $PI(4,5)P_2$ is still increased from 50 to 100 mV and that apparent saturation of $\Delta$FRET at high voltage for WT and K364M is not caused by saturation of enzyme activity. K364L showed similar profile of voltage-dependent change of F-PLC signal. The plot of $\Delta$FRET versus voltage suggests that K364I/Q/R/A showed rightward shift and K364M showed leftward shift of the $\Delta$FRET-voltage relationship along the voltage axis compared with WT (Fig. 4 *C*). Given that VSD motion did not show remarkable shift along the voltage axis in these mutants (Fig. 3 *B* and *C*), we speculate that shifts along the voltage axis of K364I/R/Q/A in the rightward direction and of K364M in the leftward direction represent weaker and stronger enzyme activity, respectively (see section "discussion").

We also estimated phosphatase activities toward $PI(4,5)P_2$ by electrophysiological measurement of GIRK2 currents. The time plot of $K_{ir}$ current magnitude (Fig. 5 *A*) was fitted by a single exponential curve (Fig. 5 *B*), and the rate constant was compared among K364 mutants and WT (Fig. 5 *C* and *D*). At the lower level of conditioning depolarization (for example, at 50 mV) of activating VSP, K364R/Q/A mutants showed less activity than WT, whereas K364M showed higher activity than WT. At 100 mV, the difference was not remarkable among mutants and WT, consistent with results of F-PLC. K364L showed similar activity to WT at all voltages, also consistent with results of F-PLC. K364I showed similar activity to WT at all voltages unlike F-PLC data, which showed slightly smaller activity than WT at 25, 50, and 75 mV.

These findings indicate that K364M showed enhanced 5-phosphatase activity against $PI(4,5)P_2$ and K364L retains similar activity to WT, whereas K364I/R/Q/A showed reduced enzyme activity with distinct magnitude among four mutants.

## Changes of the level of $PI(3,4)P_2$ in K364 mutants as reported by F-TAPP

Ci-VSP K364 mutants were coexpressed with F-TAPP, and F-TAPP FRET signal as YFP/CFP ratio was measured (Figs. 6 and S7). In Ci-VSP WT, a rapid and transient increase in FRET signal can be seen within the first second from the initiation of step pulse, representing 5-phosphate dephosphorylation of $PI(3,4,5)P_3$, which is followed by signal decline due to activity against $PI(3,4)P_2$, as previously reported (20,21). In Fig. 6 *B*, F-TAPP signal of WT and mutants was quantified by measuring the deviation of signal from the baseline at the

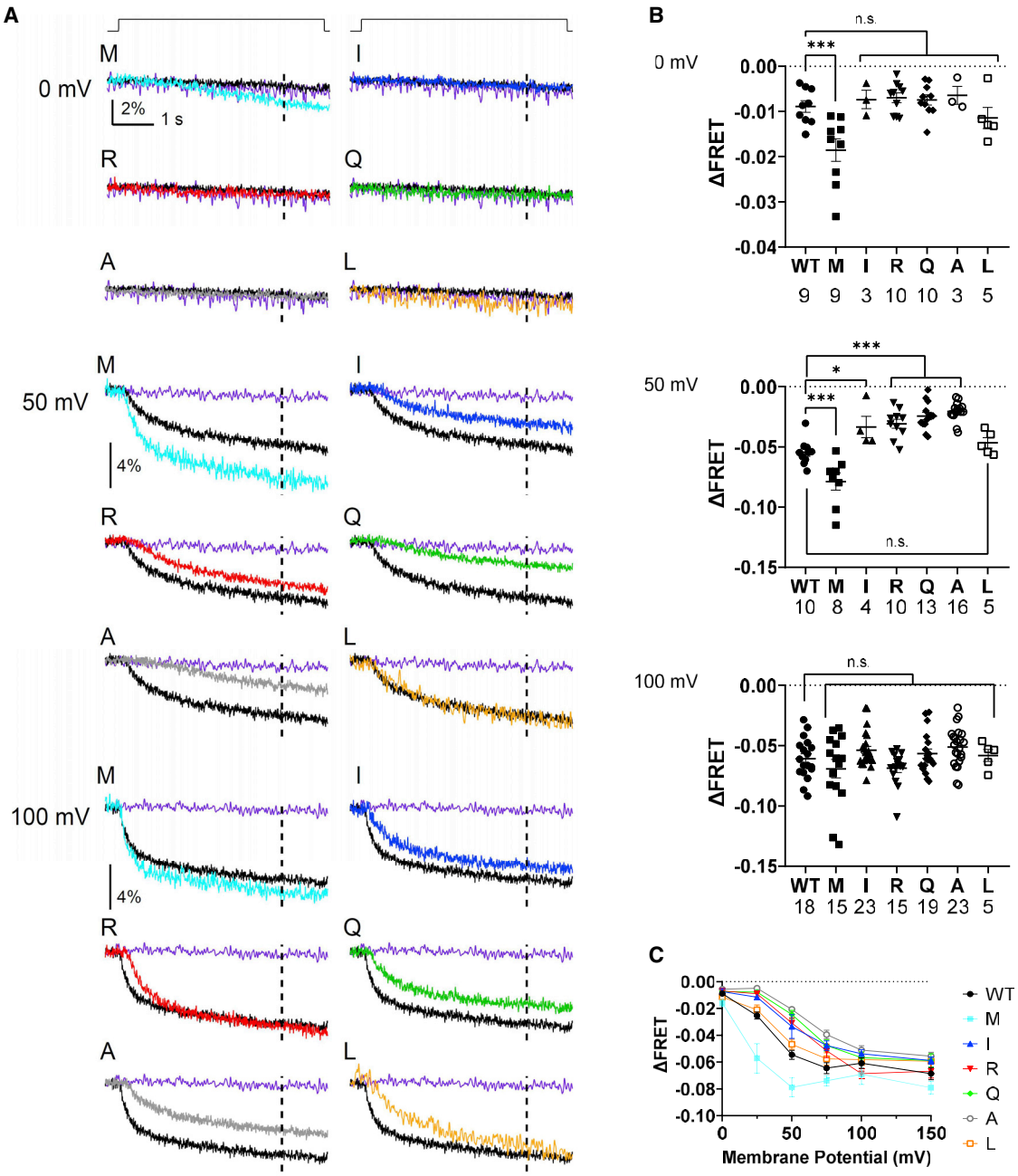


FIGURE 4 Voltage-dependent PI(4,5)$P_2$ phosphatase activity of Ci-VSP K364 mutants by VCF analysis with F-PLC, a PI(4,5)$P_2$-selective FRET probe, in *Xenopus* oocyte. (*A*) Representative traces of F-PLC YFP/CFP ratio signal measured at 0 mV (*top*), 50 mV (*middle*), and 100 mV (*bottom*). Depolarizing step shown at top of traces was applied from a holding potential of −60 mV to indicated value for 5 s. Dotted line in each trace indicates the time point (at 4 s after the beginning of depolarization) for calculating *Δ*FRET. Signal from oocytes with WT Ci-VSP and without Ci-VSP is shown as black and purple trace, respectively. (*B*) FRET signal as the shift from the baseline measured at 4 s after initiation of step at 0mV (*top*), 50 mV (*middle*), and 100 mV (*bottom*). The number of recordings is shown for WT and mutants. (*C*) Plot of deviations of standardized FRET signal from the baselines against pulse voltage. Data at 25, 75, and 150 mV are shown in Fig. S6. Each trace from 0 to 150 mV was obtained from the same oocytes. In (*B*) and (*C*), data are presented as mean ± SE. *p < 0.05; ***p < 0.001; n.s., statistically not significant, one-way ANOVA followed by Dunnett's test. Sample size is as described in (*B*) and Fig. S6 *B*.

time point of 4 s from the start of depolarization. Values represent both subreactions of PI(3,4,5)$P_3$ to PI(3,4)$P_2$, mainly at mild depolarizing levels, and of PI(3,4)$P_2$ to PI(4)P, mainly at higher depolarizing levels. In Fig. S8 *B*, to clarify the component of subreaction from PI(3,4)$P_2$ to PI(4)P, the extent of signal decrease from the peak signal at the last timing of the depolarizing step (representing subreaction of PI(3,4)$P_2$ to PI(4)P) was also plotted. Cell surface expression level of each mutant was verified by estimating $Q_{OFF}$ values by measuring off-sensing currents from the same set of cells for

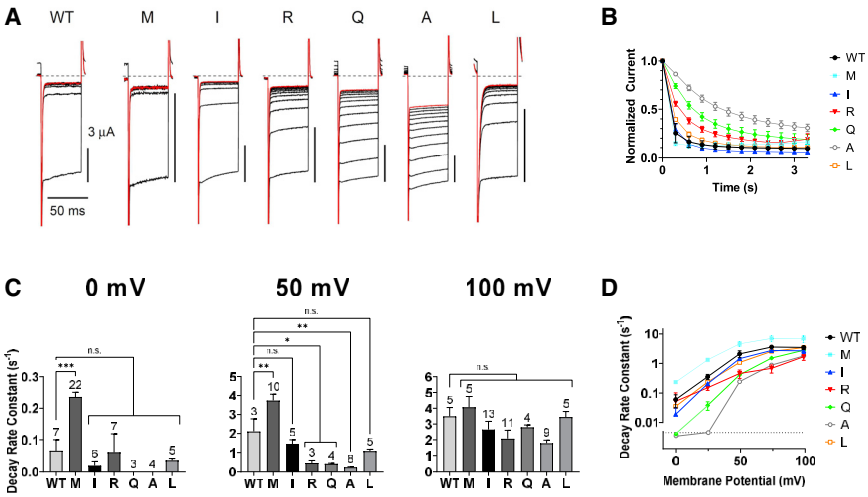


FIGURE 5 Voltage-dependent PI(4,5)$P_2$ phosphatase activity of Ci-VSP K364 mutants examined by coexpressed GIRK2 channel in *Xenopus* oocyte. (*A*) Representative GIRK2 traces followed by 50-mV depolarization. All 12 GIRK2 traces are superimposed (see also Fig. S3). The 12th traces are shown in red. Black dotted lines indicate zero current level. (*B*) Time course of GIRK2 current with conditioning depolarization to 50 mV. The current amplitudes were normalized to that in the first trace. Data are presented as mean ± SE. (*C*) Decay rate constant of the normalized GIRK2 current ($s^{-1}$) at 0 mV (*left*), 50 mV (*middle*), and 100 mV (*right*). GIRK2 was coexpressed with WT or K364 mutants. The number of recordings is shown in each bar graph. Data are presented as mean ± SE. *p < 0.05; **p < 0.01; ***p < 0.001; n.s., statistically not significant, one-way ANOVA followed by Dunnett's test. (*D*) Decay rate constant of the normalized GIRK2 current ($s^{-1}$) at different potentials. Data are presented as mean ± SE. Sample size is as described in (*C*).

recording of F-TAPP FRET signals. $Q_{OFF}$ values from all mutants were similar to that of WT (Fig. S7 *C*), suggesting that these mutants were expressed to cell membranes with a similar level to WT.

Oocytes expressing K364L, mimicking opossum VSP ortholog, showed similar profile to WT: signal increase was found at mild depolarization, whereas signals consist of early increase and late decay at higher depolarization. On the other hand, K364M, mimicking VSP ortholog of koala, Tasmanian devil, and common wombat showed more enhanced decline of the second phase, as evidenced from a remarkable downward deviation from the baseline when voltage was stepped to 25 mV (cyan trace, Fig. S7 *A*), whereas sustained signal continues over the baseline in WT (black trace, Fig. S7 *A*), indicating that K364M shows more robust 3-phosphatase activity against PI(3,4)$P_2$ than WT. Decay phase of F-TAPP signal measured at 100 and 150 mV was fitted by single exponentials, and time constant (Tau) at 150 mV was significantly smaller in K364M than in WT (Fig. 7 *A*). In contrast, four mutants, K364A/Q/R/I, showed early increase but only mild decline, and signal often did not reach the baseline level. In two methods of measurement of F-TAPP signal representing 3-phosphatase activity against PI(3,4)$P_2$ (Figs. 6, S7, and S8 *B*), results showed significantly less downward FRET signal at 50, 100, and 150 mV, suggesting that 3-phosphatase activity against PI(3,4)$P_2$ is attenuated in these K364 mutants.

Another notable finding of K364M was that the extent of F-TAPP FRET signal increase was more rapid and larger than in WT at 0 mV (Fig. 6 *A* and *B*). The slope of F-TAPP FRET signal measured at 0 mV (Fig. 7 *B*) was significantly steeper in K364M than WT, suggesting that K364M has higher 5-phosphatase activity against PI(3,4,5)$P_3$ than WT. We did not analyze the difference of 5-phosphatase activity against PI(3,4,5)$P_3$ among mutants at higher voltages, where this subreaction is partly masked by the subsequent subreaction from PI(3,4)$P_2$ to PI(4)P.

Taken together, 5-phosphatase activity against PI(3,4,5)$P_3$ and 3-phosphatase activity against PI(3,4)$P_2$ are similar in K364L to WT but more remarkable in K364M, whereas 3-phosphatase activity against PI(3,4)$P_2$ was attenuated in K364A/Q/R/I to a different degree.

Extent of 3-phosphatase activity against PI(3,4)$P_2$ and that of 5-phosphatase activity against PI(4,5)$P_2$ in the above FRET analysis were summarized at three voltages: 50, 100, and 150 mV (Fig. S8). Graphs show that 5-phosphatase activity against PI(4,5)$P_2$ and 3-phosphatase activity against PI(3,4)$P_2$ were affected in different strength. K364M showed higher 5-phosphatase activity against PI(4,5)$P_2$ (Fig. 4 *A* and *B*, 0 and 50 mV) and retained similar or slightly higher activity against PI(3,4)$P_2$ than WT (Fig. 6 *A* and *B*, 50 and 100 mV). At 100 and 150 mV, values of F-TAPP signal were variable among K364 mutants, whereas those of F-PLC signal were similar; K364M has the highest 3-phosphatase activity (F-TAPP signal), whereas K364Q and K364A showed the smallest 3-phosphatase activity against PI(3,4)$P_2$ (positive value in Fig. S8 *A* and about zero level in Fig. S8 *B*).

## Changes of the level of PI(4,5)$P_2$ by dephosphorylation of PI(3,4,5)$P_3$ by K364 mutants

We also tested 3-phosphatase activity against PI(3,4,5)$P_3$ (namely, subreaction from PI(3,4,5)$P_3$ to PI(4,5)$P_2$) by examining early rise of PI(4,5)$P_2$ level using F-PLC (13,21). However, this signal was minute even with increasing basal PI(3,4,5)$P_3$ level by insulin stimulation (25). To overcome this problem, we utilized a non-FRET-based, classical PI(4,5)$P_2$ probe, $PH_{PLC\delta}$-GFP (25). Cells

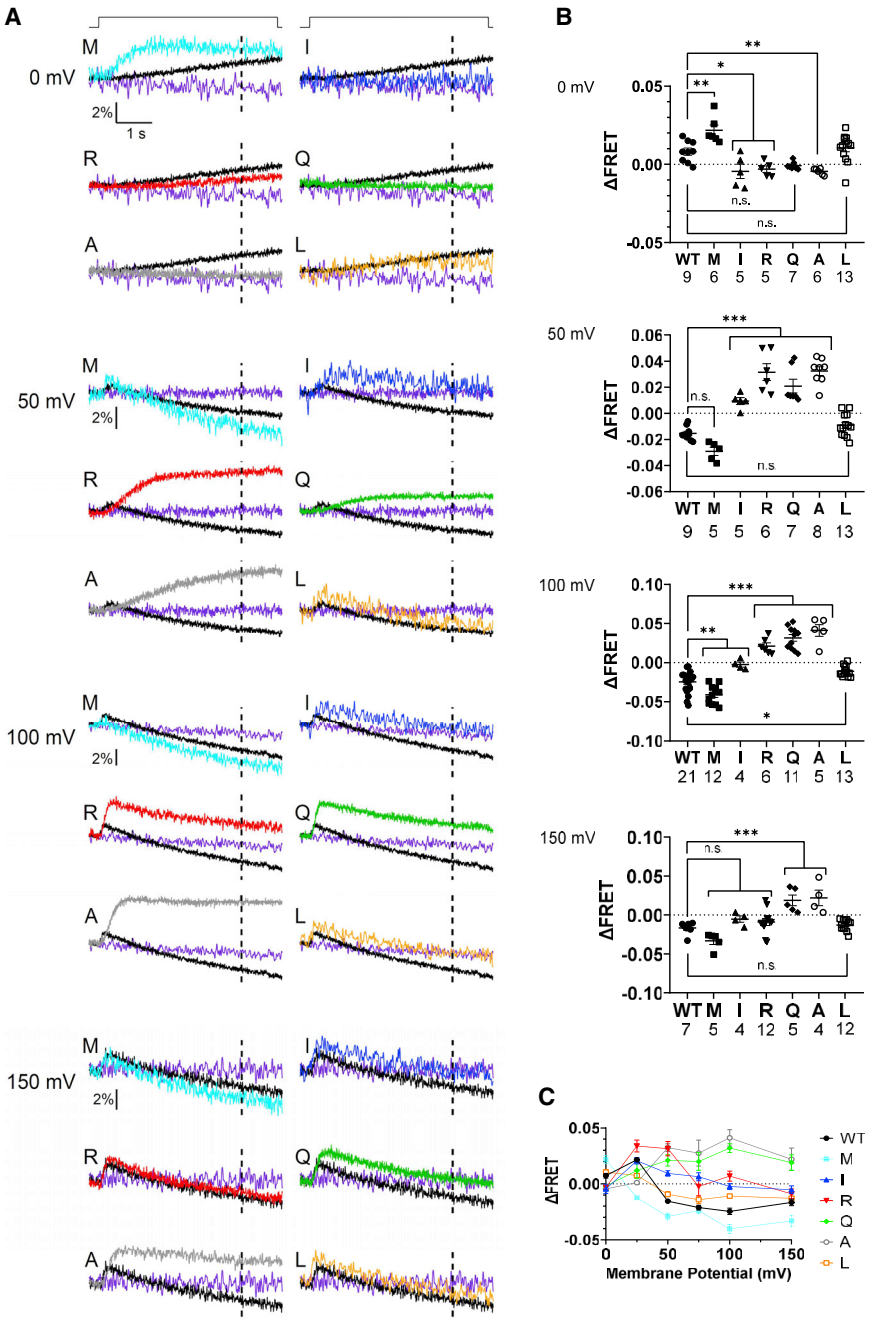


FIGURE 6 Voltage-dependent phosphatase activity by FRET analysis with F-TAPP, a $PI(3,4)P_2$ sensor in *Xenopus* oocyte. (*A*) Representative traces of F-TAPP YFP/CFP ratio signal measured at 0, 50, 100, and 150 mV from top to bottom. Depolarizing step shown at top of traces was applied from a holding potential of −60 mV to indicated value for 5 s. Dotted line in each trace indicates the time point (at 4 s after the beginning of depolarization) for calculating *Δ*FRET. Signal from oocytes with WT Ci-VSP and without Ci-VSP is shown as black and purple trace, respectively. (*B*) FRET signal as the shift from the baseline measured at 4 s after initiation of step to 0, 50, 100, and 150 mV from top to bottom. The number of recordings is shown for WT and mutants. Data are presented as mean ± SE. (*C*) Decrease of FRET signal at 4 s after initiation of voltage step for each mutant plotted against voltage. Data at 25 and 75 mV are shown in Fig. S6. Each trace from 0 to 150 mV was obtained from the same oocytes. In (*B*) and (*C*), data are presented as mean ± SE. *p < 0.05; **p < 0.01; ***p < 0.001; n.s., statistically not significant, one-way ANOVA followed by Dunnett's test. Sample size is as described in (*B*) and Fig. S7 *B*.

were preincubated with insulin for 10 min followed by VCF measurements. Results showed that all mutants exhibited clear transient increase of signal of $PH_{PLC\delta}$-GFP upon membrane depolarization (Fig. S9), representing earlier activity of dephosphorylation of $PI(3,4,5)P_3$ into $PI(4,5)P_2$ followed by dephosphorylation of $PI(4,5)P_2$ into PI(4)P. Variabilities of signal magnitude (*Δ*F/F) were too large among cells to quantitatively compare magnitude of activity from $PI(3,4,5)P_3$ to $PI(4,5)P_2$ among mutants. Within this limited resolution, we could not detect a significant difference in the rise of $PH_{PLC\delta}$-GFP signal among WT and mutants, suggesting that K364 mutation does not affect 3-phosphatase activity against $PI(3,4,5)P_3$.

## Malachite green assay showed no remarkable difference among WT and K364 mutants, K364 M/L/R

We compared substrate specificity of K364 mutants, K364 M/L/R, in vitro by using malachite green assay, a colorimetric assay that changes color in the presence of free phosphate with BIOMOL Green following our previous

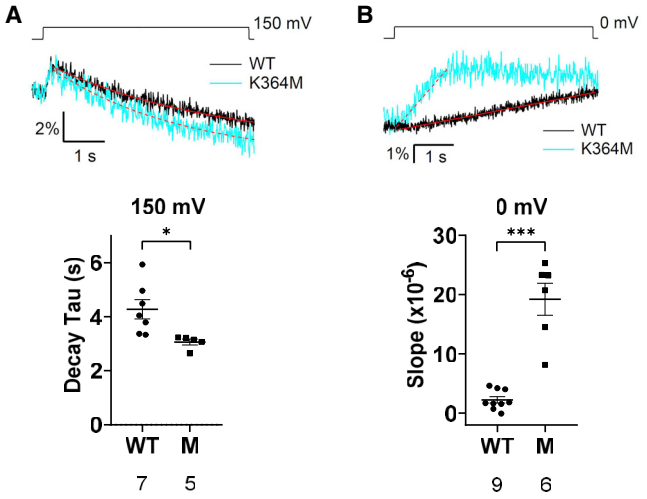


FIGURE 7 Phosphatase activity against $PI(3,4,5)P_3$ to $PI(3,4)P_2$ at 0 mV and $PI(3,4)P_2$ to PI(4)P at 150 mV in Ci-VSP K364M mutant in *Xenopus* oocyte. (*A*) Representative traces of F-TAPP FRET signal of WT and K364M measured at 150 mV (*top*). At 150 mV, the decrease of $PI(3,4)P_2$ representing the subreaction against $PI(3,4)P_2$ is more manifested than the increase of $PI(3,4)P_2$ representing the reaction of dephosphorylation of $PI(3,4,5)P_3$. The same traces are shown in Fig. 6 *A*. Solid and dotted lines colored red indicate single exponential fitting for traces of WT and K364M, respectively. Each decay Tau calculated by single exponential fitting for F-TAPP signal during depolarization was plotted on a graph for evaluating the subreaction from $PI(3,4)P_2$ to PI(4)P (*bottom*). (*B*) Representative traces of F-TAPP FRET signal of WT and K364M measured at 0 mV (*top*). The same traces are shown in Fig. 6 *A*. At 0 mV, the increase of $PI(3,4)P_2$ representing the reaction of dephosphorylation of $PI(3,4,5)P_3$ is more manifested than the decrease of $PI(3,4)P_2$ representing the subreaction against $PI(3,4)P_2$. Solid and dotted lines colored red indicate linear fitting for traces of WT and K364M, respectively. Each slope calculated by linear fitting for F-TAPP signal during depolarization was plotted on a graph for evaluating the subreaction from $PI(3,4,5)P_3$ to $PI(3,4)P_2$ (*bottom*). For K364M, the slope was calculated by fitting from the point starting depolarization to peak. Data are presented as mean ± SE. *p < 0.05, ***p < 0.001, two-tailed unpaired *t*-test.

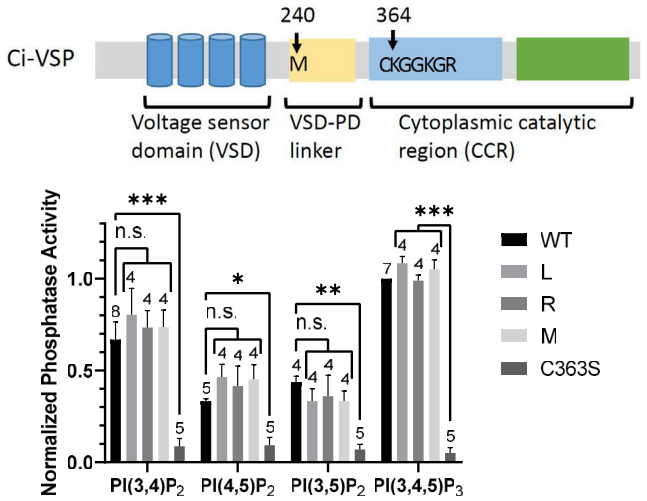


FIGURE 8 In vitro malachite green assay of the CCR of K364 mutants (K364M/L/R) of Ci-VSP. Schematic primary structure of Ci-VSP with position of M240 and the enzyme active center region containing $Cx_5R$ motif (*top*). M240 is N terminus of the proteins synthesized for malachite green assay. Malachite green assay absorbance at 660 nm for different mutants (*bottom*). Data were normalized to the values of WT Ci-VSP's activity with $PI(3,4,5)P_3$ as substrate. Data are presented as mean ± SE. *p < 0.05; **p < 0.01; ***p < 0.001; n.s., statistically not significant, one-way ANOVA followed by Dunnett's test. Statistics were analyzed between WT and mutants for three kinds of $PIP_2$ and between C363S and K364 mutants for $PI(3,4,5)P_3$. Number of experiment is shown above each bar graph.

research in which the polypeptide consisting of the CCR of Ci-VSP was incubated with target PIPs (17,24). Polypeptides of Ci-VSP segment 240–576 and its mutants (L, R, M, and C363S), corresponding to the entire C-terminal cytoplasmic region, which were purified after synthesis in *Escherichia coli*, were used. Malachite green assay did not show significant activity change among WT and mutants (Fig. 8).

## Dr-VSP with K303M mutation corresponding to K364M Ci-VSP shows slightly increased voltage-dependent phosphatase activity against $PI(4,5)P_2$

The above results suggest that K364M mutant Ci-VSP showed more robust 5-phosphatase activity against $PI(4,5)P_2$ and $PI(3,4,5)P_3$. Dr-VSP has often been utilized as a molecular tool to study $PI(4,5)P_2$-sensitive activities of ion channels or transporters in mammalian cells (6,34). Guided by our findings of Ci-VSP K364M mutant, we tested whether our previously developed *e*VSP (Dr-VSP with mutation in the hydrophobic spine, L223F) could be further modified by introduction of single amino acid mutation of K303M which corresponds to amino acid change of K364M in Ci-VSP or naturally occurs in several mammals.

Voltage-dependent $PI(4,5)P_2$ phosphatase activity was compared between L223F (*e*VSP) and L223F/K303M in HEK293T cells by coexpressing KCNQ2/3 channel, which is highly sensitive to $PI(4,5)P_2$ (35,36). With repeated depolarizing stimuli, KCNQ2/3 activity as examined by the magnitude of outward current measured at the end of a 300-ms test pulse to 0 mV did not decrease at all when VSP was spared (data not shown), whereas it gradually decreased upon coexpression with *e*VSP and L223F/K303M. Speed of decline becomes accelerated as interval voltage is higher (Fig. 9 *A*). Decline speed is significantly faster in L223F/K303M than *e*VSP at two voltages (0 and 25 mV) (Fig. 9 *B*). These are consistent with the idea that K303M mutation increased 5-phosphatase activity toward $PI(4,5)P_2$. In a different set of cells, we measured sensing currents, and the $Q_{OFF}$-$V$ curve showed no shift of voltage dependence of voltage sensor motion. Maximum sensing charges measured at 200 mV were slightly reduced in K303M (0.86 ± 0.36 nC (n = 7) and 1.69 ± 0.98 nC (n = 5) for L223F/K303M and *e*VSP, respectively), suggesting that increased phosphatase activity in K303M is slightly underestimated in this experiment.

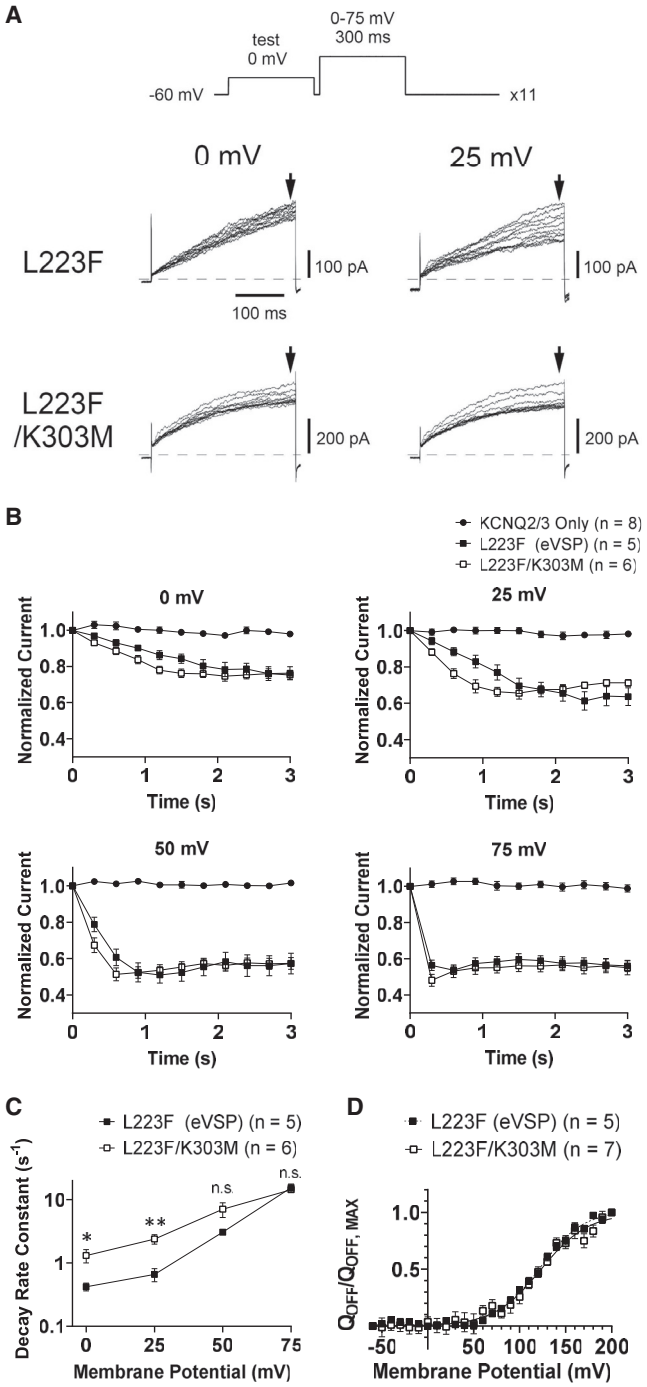


FIGURE 9 An enhanced version of Dr-VSP by mutation of K to M in the background of *e*VSP (Dr-VSP L223F). Enhanced voltage-dependent $PI(4,5)P_2$ phosphatase activity shown by measuring activities of KCNQ2/3 channels in HEK293T cells. (*A*) Representative KCNQ2/3 current traces in HEK293T cells expressing L223F (*e*VSP) and L223F/K303M mutant when the membrane was depolarized to 0 and 25 mV. The pulse protocol is shown in the top panel. All 11 traces recorded during the test pulse are superimposed. Dotted lines indicate zero current level. (*B*) Time-dependent change of the magnitude of KCNQ2/3 current at the end of the test pulse (arrows in *A*) with conditioning depolarization to 0, 25, 50, and 75 mV. The current amplitudes were normalized to that in the first trace. (*C*) Decay rate constant of normalized KCNQ2/3 current was plotted against membrane potential. KCNQ2/3 were coexpressed with L223F (*e*VSP) or L223F/K303M. Decay rate constant was acquired as rate constant of decay time course of KCNQ2/3 fitted with single exponential function. *$p < 0.05$; **$p < 0.01$; n.s., statistically not significant, two-tailed unpaired *t*-test. (*D*) Normalized charge was plotted against membrane potential. $Q_{OFF}$-V curves were fitted with the Boltzmann equation: $Q_{OFF}(V)/Q_{MAX} = 1/[1 + exp(-ZF(V\text{-}V_{Half})/RT)]$, where *F* is Faraday constant, *R* is the gas constant, *T* is the absolute temperature, *Z* is the effective valency, V is voltage, and $V_{Half}$ is the voltage that gives half of the maximum $Q_{OFF}$ ($Q_{MAX}$). Values of ($V_{Half}$, Z) are (122.9 ± 1.3 mV, 1.0) and (122.0 ± 0.8 mV, 1.1) for L223F/K303M and L223F (*e*VSP), respectively. Black curve, L223F/K303M; black dotted curve, L223F (*e*VSP). In (*B*) to (*D*), data are presented as mean ± SE.

## DISCUSSION

The VSP gene is evolutionarily conserved and found widely from marine invertebrates to mammals. By extensive database search for amino acid sequences of numerous putative VSP orthologs, we found that VSP orthologs from several mammals showed diversity at the lysine residue of the $Cx_5R$ motif, one amino acid from the active site cysteine. Since the corresponding site in PTEN is known to be critical for phosphatase activity toward $PI(3,4,5)P_3$, we examined impact of mutation of K364 in Ci-VSP on voltage-dependent phosphatase activities by monitoring $PI(4,5)P_2$ and $PI(3,4)P_2$ using *Xenopus* oocyte expression system. Different Ci-VSP mutants with K364 replaced by different amino acids showed a wide spectrum of changes in both 5-phosphastase activity toward $PI(4,5)P_2$ and 3-phosphatase activity toward $PI(3,4)P_2$. Mutation mimicking mutation of Ci-VSP K364M in Dr-VSP (K303M *e*VSP) led to slightly increased ability of depleting $PI(4,5)P_2$ in HEK293T cells.

### Apparent shift of voltage dependence of enzyme activity among K364 mutants

In our study, F-PLC fluorescence change, ΔFRET, plotted as different voltages showed unexpected shift of voltage dependence with similar maximum magnitude of ΔFRET change among K364 mutants (Fig. 4 *C*). It is clear that such shift does not derive from altered nature of VSD, since fluorescence change based on voltage sensor motion in VCF experiments showed little shift of $V_{Half}$ value among WT and K364 mutants (Fig. 3). We interpret that ΔFRET value at high voltage is slightly deviated from what could be expected from actual enzyme activity. For example, K364M showed more rapid kinetics of F-PLC signal at 100 mV than at 50 mV (Fig. 4 *A*), suggesting that enzyme activity is higher at 100 mV than at 50 mV, whereas ΔFRET value was similar between 50 and 100 mV. This may be in part due to possible insufficient linearity of F-PLC FRET signal in a range of low concentration of $PI(4,5)P_2$ or alternatively due to overlapping background signal, which might exceed F-PLC fluorescence upon $PI(4,5)P_2$ depletion.

## Roles of K364 within $Cx_5R$ and insights into 3-phosphastase and 5-phosphatase activity of VSP

The trial of functional characterization of opossum VSP with native amino acid sequence in a heterologous expression system was unsuccessful most likely due to insufficient cell surface expression. Chimera experiment of sea squirt (*C. intestinalis*) and opossum VSP was partially successful, but cell surface expression was not robust. Therefore, we took a strategy of making mutation into Ci-VSP, and made several mutants including naturally occurring amino acid change such as K to M (mimicking Tasmanian devil, prairie deer mouse, koala, and common wombat) and K to L (mimicking short-tailed opossum). It is known that VSP mediates at least four subreactions based on 3-phosphatase activity toward $PI(3,4,5)P_3$ and $PI(3,4)P_2$ and 5-phosphatase activity toward $PI(3,4,5)P_3$ and $PI(4,5)P_2$ (6,13). In this study, enzyme activities were analyzed using $PI(4,5)P_2$ or $PI(3,4)P_2$ selective FRET sensors in *Xenopus* oocyte. We also made semi-quantitative comparison of 3-phosphatase activities toward $PI(3,4,5)P_3$ (subreaction from $PI(3,4,5)P_3$ to $PI(4,5)P_2$) among mutants using a single chromophore probe sensitive to $PI(4,5)P_2$, the GFP-fused PH domain derived from PLC-$\delta$.

The results of K364 mutants of Ci-VSP showed a fairly wide spectrum of changes of 3-phosphatase activity toward $PI(3,4)P_2$ and 5-phosphatase activity toward $PI(4,5)P_2$. K364L showed similar magnitude of both activities to WT. Compared with WT, K364M mutant showed more remarkable 5-phosphatase activity against $PI(4,5)P_2$ and $PI(3,4,5)P_3$ and 3-phosphatase activity against $PI(3,4)P_2$. The other four mutants, K364I/R/A/Q, shared phenotypes; they showed mild reduction of 5-phosphatase activity toward $PI(4,5)P_2$ with distinct extent and only mild decline of $PI(3,4)P_2$ level at high voltage in contrast with WT, suggesting reduced dephosphorylation of 3-phosphate from $PI(3,4)P_2$. Experiments with $PH_{PLC\delta}$-GFP to study subreaction of dephosphorylation of $PI(3,4,5)P_3$ showed clear signal rise at lower voltage, reflecting dephosphorylation of 5-phosphate from $PI(3,4,5)P_3$ in all mutants. These indicate that K364 is not indispensable for 3-phosphatase activity against both $PI(3,4)P_2$ and $PI(3,4,5)P_3$. Ideally, to evaluate the impact of amino acid mutation at K364 on phosphatase activity may require a cell-free reconstitution system with known concentration of PIPs at the resting state, since the heterologous cell expression system has limitations in control of initial concentrations of substrate PIPs before activation of VSP. Nevertheless, future study similar to modeling analysis of F-PLC and F-TAPP FRET data measured in heterologous cell expression systems (13,22) will provide deeper insights into the role of K364 in substrate preference of VSP.

It is clear that results are more complicated than what could be mechanistically explained by physico-chemical natures of amino acid residues, such as hydrophobicity or charge or side chain length. For example, K364R, which retains the positive charge, showed significantly weaker 3-phosphatase activity against $PI(3,4)P_2$ than WT. K364I showed significantly weaker 3-phosphatase activity against $PI(3,4)P_2$ than K364L. K364M showed more robust enzyme activity than WT. In PTEN, mutation of K125, a site corresponding to K364 of Ci-VSP, remarkably reduces phosphatase activity to $PI(3,4,5)P_3$ (18) and some human cancer patients show amino acid replacement at this site (COSMIC database). However, there is no information available about protein structure with substrate bound to PTEN and molecular mechanisms underlying the role of K125 in PTEN still remain unclear. In the paper by Lee et al., activity toward p-nitrophenyl phosphate, a nonspecific substrate, was also reduced by K125 mutation (18). Most of the K364 mutants of Ci-VSP showed robust phosphatase activities in our results, indicating that the role of K364 in VSP is not comparable to that of K125 in PTEN. No clear relationship between phenotypes and the physico-chemical nature of amino acids introduced at K364 suggests that K364 is not directly involved in recognizing headgroup of PIPs. This is consistent with the fact that lysine is also conserved in the corresponding site of the $Cx_5R$ motif of other phosphatases that do not dephosphorylate 3-phosphate on the inositol ring, including type I inositol-3,4-bisphosphate 4-phosphatase and PLIP, a PTEN-related 5-phosphatidy linositol phosphatase localized in the Golgi.

## Interplay between VSD and enzyme active site

We found that K364M showed slower kinetics by VCF measurements. K364L showed a slight shift of the F-V curve, in particular at higher voltage. It has been shown that G214C-TMRM signal represents both S4 motion and the state of the entire VSD, which is called relaxation (37,38). Previous reports showed that kinetics of G214C-TMRM signal became slower when mutation was introduced at C363, which is the critical site for enzyme reaction (39). However, slow kinetics of K364M observed in our study of G214C-TMRM fluorometry is more remarkable than in the case with C363S. These findings suggest that increased voltage-dependent enzyme activities of K364M as seen by FRET probes in this study is due to enhanced coupling between VSD and the enzyme region, since in vitro malachite green assay of the isolated CCR did not show any significant difference of robustness or substrate preferences between K364M and WT.

This accelerated coupling in K364M could be mediated by the allosteric effect by the specific nature of methionine at position 364. Regarding K364I and K364R mutants, there was also an unexpected gap between FRET measurements of voltage-dependent phosphatase activities and malachite green assay; both mutants showed weaker 5-phosphatase activity against $PI(4,5)P_2$ and 3-phosphatase activity against

$PI(3,4)P_2$ than WT, whereas their malachite green assay results did not show any significant difference from WT. These phenotypes of K364I and K364R expressed in *Xenopus* oocyte may be accounted for by weakened coupling between VSD and enzyme binding site. Since the position of K364 is remote from the VSD, we do not know how amino acid change of K364 can interplay with VSD. Hydrophobic transmembrane segments may interact with acyl-chain of PIPs, and voltage-induced alteration of orientation of transmembrane regions, in particular S4, may bias substrate binding or turnover rate through interaction with acyl-group of PIPs. This issue needs detailed structural analysis or MD simulation under electric field across membrane in the future.

### Significance of amino acid diversity at K364 position among mammals; role of VSP in sperm and epithelium

Ci-VSP with K364L, which mimics amino acid change in short-tailed opossum, showed similar phosphatase activities to WT. Ci-VSP K364M, which mimics K to M change in the orthologs of Tasmanian devil, koala, prairie deer mouse, and common wombat, showed increased activity of 5-phosphatase against $PI(3,4,5)P_3$ and $PI(4,5)P_2$ and 3-phosphatase against $PI(3,4)P_2$. When K364 was replaced by Q, I, L, and A, 3-phosphatase activity toward $PI(3,4)P_2$ was decreased, as seen by F-TAPP measurement. It is intriguing that, among all tested amino acid species at the K364 position, only methionine and leucine, which gave potent voltage-dependent 3-phosphatase activities, are naturally found in mammals. In addition, our preliminary experiment showed that mutation of K364N, which mimics amino acid change in the northern gibbon VSP ortholog, did not significantly affect either 5-phosphatase or 3-phosphatase activities.

In this study, we learned that VSP orthologs have highly conserved 3-phosphatase activities across animal species. In sea squirt, mouse, and human, VSP is expressed most abundantly in spermatocytes. Sperm of VSP-knockout mice shows insufficient in vitro fertilization due to abnormal maturation of sperm function. This depends on VSP's regulation of $PI(4,5)P_2$ on sperm flagellum membrane (8). On the other hand, zebrafish VSP is expressed in endomembranes of gut epithelial cells, and knockout fish exhibit defects of endocytosis (40). In endomembranes such as endo/lysosomes or autophagosomes, several 3-phosphatases, such as myotubularins, play key roles, suggesting that 3-phsophatase activity of VSP may be important in functions in those epithelial cells. In mammals, ileum at the preweaning stage contains similar epithelial cells that harbor activities of endocytosis for nutrient transport (41). It is possible that both 3- and 5-phosphatase activities play critical roles in enterocytes in mammals besides the function of 5-phosphatase activities in sperm. During evolution of mammalian species, which have methionine instead of lysine at the corresponding site of Ci-VSP K364, amino acid change from K to M was probably more favorable for survival for its higher efficiency of coupling between VSD and enzyme. This view can explain why amino acid diversity at this position is not restricted to marsupials, which live in restricted areas in the world, but in a wider range species of mammals, such as rodents (prairie deer mouse). Future analysis of full-length mammalian VSP orthologs expressed in heterologous expression, other amino acid mutations, in the model VSP such as Ci-VSP, and further emerging genome information of a wider range of species will lead to gain more insights into the physiological significance of amino acid diversity at this position in $Cx_5R$.

### VSP as a molecular tool

VSP has been utilized as a molecular tool to acutely deplete $PI(4,5)P_2$ in heterologous expression systems (6,34,42). An advantage of VSP as such a tool, in contrast with other molecular tools for studying PIPs in biology, is that depletion with VSP is acute and reversible. We previously engineered Dr-VSP by improving restriction of expression to the cell surface as well as improving coupling efficiency between VSD and CCR based on biophysical mechanisms of coupling (26,29). In this study, based on information of biodiversity at the K364 (Ci-VSP) position, we modified a previously established *e*VSP (a version of Dr-VSP with K303M mutation with enhanced cell surface expression) by mimicking Ci-VSP K364M. It showed more remarkable 5-phosphatase activity toward $PI(4,5)P_2$ than *e*VSP. It is intriguing that the effect of K364M mutation in Ci-VSP seems shared by Dr-VSP, despite the voltage range of activation of VSD being largely shifted (42). Whether K303M mutation in Dr-VSP increases 3-phosphatase activity as K364M mutation in Ci-VSP still remains yet to be determined. Detailed comparison among VSP orthologs may be helpful in the future to elucidate molecular mechanisms for how 5-phosphatase and 3-phosphatase are regulated in VSP. This will also make further customization of a VSP-based tool possible for future PIP biology and biophysics.

## CONCLUSIONS

The lysine residue next to the active site cysteine of the $Cx_5R$ motif, conserved also in PTEN, is diversified in several mammalian VSP orthologs. Two K364 mutants of Ci-VSP mimicking these mammalian VSP orthologs, K364L and K364M, showed similar or higher enzyme activity than WT and still retained 3-phosphatase activity, indicating that roles of positive charge at this site in 3-phosphatase activity differ from those of PTEN where lysine at the corresponding site is essential for its enzyme activity. Despite enhanced voltage-dependent enzyme

activity of K364M expressed in *Xenopus* oocyte, measurements of in vitro malachite green assay with isolated CCR region of K364M showed no change of phosphatase activities from WT, suggesting K364M mutation facilitates interaction between the VSD and the enzyme active center. These findings were exploited to enhance voltage-dependent enzyme activity of a version of Dr-VSP as a molecular tool for transiently depleting $PI(4,5)P_2$ in mammalian cells.

## SUPPORTING MATERIAL

Supporting material can be found online at https://doi.org/10.1016/j.bpj.2023.01.022.

## AUTHOR CONTRIBUTIONS

All authors contributed to the preparation of the manuscript. Yasushi Okamura, T.K., and Yoshifumi Okochi designed the research. I.P. performed most of the experiments and data analysis, including molecular biological experiments, the electrophysiological experiments in *Xenopus* oocyte, and the malachite green assay. N.M. verified plasmid constructions, performed molecular biological experiments and electrophysiological experiments in oocytes and HEK293T cells, analyzed data, and helped I.P. to conduct electrophysiological experiments in oocytes. M.M. prepared protein constructs for malachite green assay and helped I.P. to perform the assay. R.A. performed molecular biological and electrophysiological experiments in oocytes. Yoshifumi Okochi supervised molecular biological experiments, malachite green assay, and data analysis. T.K. helped I.P. to perform electrophysiological studies and data analysis. A.N. conducted data interpretation from aspects of protein structures. I.P., Yasushi Okamura, and Yoshifumi Okochi wrote the paper, and all authors approved the final version. This work was conducted as a partial fulfillment of the Master thesis of I.P.

## ACKNOWLEDGMENTS

We thank Dr. Ehud Isacoff (UC Berkeley) for providing F-PLC and F-TAPP plasmids, Dr. Takushi Shimomura (National Institute for Physiological Sciences, Japan), and Dr. Akira Kawanabe (Kagawa University, Japan) for their invaluable advice. We would also like to thank Dr. Hiroshi Kiyonari at the RIKEN Center for Biosystems Dynamics Research at Kobe Riken for providing a sample of opossum. We would also like to thank all Okamura lab members for their insightful discussion. Natsuki Mizutani was supported by the Honjo International Scholarship Foundation as the 25th scholarship student. This work was supported by the Ministry of Education, Culture, Sports, Science and Technology (MEXT) Grant-in-Aid for Scientific Research on Innovative Areas (JP15H05901 and JP22H02804 to Yasushi Okamura); Japan Society for the Promotion of Science (JSPS), KAKENHI (JP19H03401 to Yasushi Okamura, and JP21H02444 to Atsushi Nakagawa); Japan Science and Technology Agency (JST), CREST (JPMJCR14M3 to Atsushi Nakagawa and Yasushi Okamura); and the Mitsubishi Foundation and the Japan Foundation for Applied Enzymology (to Yasushi Okamura).

## DECLARATION OF INTERESTS

The authors declare that they have no known competing financial interests or professional relationship with other organizations, or with the people working with them, that could influence their research.

## REFERENCES

1. Hilgemann, D. W., S. Feng, and C. Nasuhoglu. 2001. The complex and intriguing lives of PIP2 with ion channels and transporters. *Sci. Signal.* 2001:re19.
2. Yen, H. Y., K. K. Hoi, …, C. V. Robinson. 2018. PtdIns(4,5)P2 stabilizes active states of GPCRs and enhances selectivity of G-protein coupling. *Nature.* 559:423–427.
3. Karathanassis, D., R. V. Stahelin, …, R. L. Williams. 2002. Binding of the PX domain of p47phox to phosphatidylinositol 3,4-bisphosphate and phosphatidic acid is masked by an intramolecular interaction. *EMBO J.* 21:5057–5068.
4. Balla, T. 2013. Phosphoinositides: tiny lipids with giant impact on cell regulation. *Physiol. Rev.* 93:1019–1137.
5. Hammond, G. R. V., and J. E. Burke. 2020. Novel roles of phosphoinositides in signaling, lipid transport, and disease. *Curr. Opin. Cell Biol.* 63:57–67.
6. Okamura, Y., A. Kawanabe, and T. Kawai. 2018. Voltage-sensing phosphatases: biophysics, physiology, and molecular engineering. *Physiol. Rev.* 98:2097–2131.
7. Mizutani, N., A. Kawanabe, …, Y. Okamura. 2022. Interaction between S4 and the phosphatase domain mediates electrochemical coupling in voltage-sensing phosphatase (VSP). *Proc. Natl. Acad. Sci. USA.* 119:e2200364119.
8. Kawai, T., H. Miyata, …, Y. Okamura. 2019. Polarized PtdIns(4,5)P2 distribution mediated by a voltage-sensing phosphatase (VSP) regulates sperm motility. *Proc. Natl. Acad. Sci. USA.* 116:26020–26028.
9. Tsutsui, H., N. Mizutani, and Y. Okamura. 2021. Engineering voltage sensing phosphatase (VSP). *Methods Enzymol.* 654:85–114.
10. Doumane, M., M. C. Caillaud, and Y. Jaillais. 2022. Experimental manipulation of phosphoinositide lipids: from cells to organisms. *Trends Cell Biol.* 32:445–461.
11. Kurokawa, T., S. Takasuga, …, Y. Okamura. 2012. 3' Phosphatase activity toward phosphatidylinositol 3,4-bisphosphate [PI(3,4)P2] by voltage-sensing phosphatase (VSP). *Proc. Natl. Acad. Sci. USA.* 109:10089–10094.
12. Liu, L., S. C. Kohout, …, D. L. Minor. 2012. A glutamate switch controls voltage-sensitive phosphatase function. *Nat. Struct. Mol. Biol.* 19:633–641.
13. Keum, D., M. Kruse, …, B. C. Suh. 2016. Phosphoinositide 5- and 3-phosphatase activities of a voltage-sensing phosphatase in living cells show identical voltage dependence. *Proc. Natl. Acad. Sci. USA.* 113:E3686–E3695.
14. Halaszovich, C. R., M. G. Leitner, …, D. Oliver. 2012. A human phospholipid phosphatase activated by a transmembrane control module. *J. Lipid Res.* 53:2266–2274.
15. Lacroix, J., C. R. Halaszovich, …, C. A. Villalba-Galea. 2011. Controlling the activity of a phosphatase and tensin homolog (PTEN) by membrane potential. *J. Biol. Chem.* 286:17945–17953.
16. Iwasaki, H., Y. Murata, …, Y. Okamura. 2008. A voltage-sensing phosphatase, Ci-VSP, which shares sequence identity with PTEN, dephosphorylates phosphatidylinositol 4,5-bisphosphate. *Proc. Natl. Acad. Sci. USA.* 105:7970–7975.
17. Matsuda, M., K. Takeshita, …, A. Nakagawa. 2011. Crystal structure of the cytoplasmic phosphatase and tensin homolog (PTEN)-like region of Ciona intestinalis voltage-sensing phosphatase provides insight into substrate specificity and redox regulation of the phosphoinositide phosphatase activity. *J. Biol. Chem.* 286:23368–23377.
18. Lee, J. O., H. Yang, …, N. P. Pavletich. 1999. Crystal structure of the PTEN tumor suppressor: implications for its phosphoinositide phosphatase activity and membrane association. *Cell.* 99:323–334.
19. Leitner, M. G., K. Hobiger, …, C. R. Halaszovich. 2018. A126 in the active site and TI167/168 in the TI loop are essential determinants of the substrate specificity of PTEN. *Cell. Mol. Life Sci.* 75:4235–4250.

20. Rayaprolu, V., P. Royal, …, S. C. Kohout. 2018. Dimerization of the voltage-sensing phosphatase controls its voltage-sensing and catalytic activity. *J. Gen. Physiol.* 150:683–696.

21. Grimm, S. S., and E. Y. Isacoff. 2016. Allosteric substrate switching in a voltage-sensing lipid phosphatase. *Nat. Chem. Biol.* 12:261–267.

22. Kruse, M., S. C. Kohout, and B. Hille. 2019. Reinterpretation of the substrate specificity of the voltage-sensing phosphatase during dimerization. *J. Gen. Physiol.* 151:258–263.

23. Mavrantoni, A., V. Thallmair, …, C. R. Halaszovich. 2015. A method to control phosphoinositides and to analyze PTEN function in living cells using voltage sensitive phosphatases. *Front. Pharmacol.* 6:68.

24. Murata, Y., H. Iwasaki, …, Y. Okamura. 2005. Phosphoinositide phosphatase activity coupled to an intrinsic voltage sensor. *Nature.* 435:1239–1243.

25. Murata, Y., and Y. Okamura. 2007. Depolarization activates the phosphoinositide phosphatase Ci-VSP, as detected in Xenopus oocytes coexpressing sensors of PIP2. *J. Physiol.* 583:875–889.

26. Kawanabe, A., N. Mizutani, …, Y. Okamura. 2020. Engineering an enhanced voltage-sensing phosphatase. *J. Gen. Physiol.* 152:e201912491.

27. Kumar, S., G. Stecher, …, K. Tamura. 2018. Mega X: molecular evolutionary genetics analysis across computing platforms. *Mol. Biol. Evol.* 35:1547–1549.

28. Kohout, S. C., M. H. Ulbrich, …, E. Y. Isacoff. 2008. Subunit organization and functional transitions in Ci-VSP. *Nat. Struct. Mol. Biol.* 15:106–108.

29. Kawanabe, A., M. Hashimoto, …, Y. Okamura. 2018. The hydrophobic nature of a novel membrane interface regulates the enzyme activity of a voltage-sensing phosphatase. *Elife.* 7:e41653.

30. Pagliarini, D. J., C. A. Worby, and J. E. Dixon. 2004. A PTEN-like phosphatase with a novel substrate specificity. *J. Biol. Chem.* 279:38590–38596.

31. Hossain, M. I., H. Iwasaki, …, Y. Okamura. 2008. Enzyme domain affects the movement of the voltage sensor in ascidian and zebrafish voltage-sensing phosphatases. *J. Biol. Chem.* 283:18248–18259.

32. Rosasco, M. G., S. E. Gordon, and S. M. Bajjalieh. 2015. Characterization of the functional domains of a mammalian voltage-sensitive phosphatase. *Biophys. J.* 109:2480–2491.

33. Walker, S. M., C. P. Downes, and N. R. Leslie. 2001. TPIP: a novel phosphoinositide 3-phosphatase. *Biochem. J.* 360:277–283.

34. Falkenburger, B. H., J. B. Jensen, and B. Hille. 2010. Kinetics of PIP 2 metabolism and KCNQ2/3; channel regulation studied with a voltage-sensitive phosphatase in living cells. *J. Gen. Physiol.* 135:99–114.

35. Suh, B. C., T. Inoue, …, B. Hille. 2006. Rapid chemically induced changes of PtdIns(4,5)P2 gate KCNQ ion channels. *Science.* 314:1454–1457.

36. Delmas, P., and D. A. Brown. 2005. Pathways modulating neural KCNQ/M (Kv7) potassium channels. *Nat. Rev. Neurosci.* 6:850–862.

37. Villalba-Galea, C. A., W. Sandtner, …, F. Bezanilla. 2009. Charge movement of a voltage-sensitive fluorescent protein. *Biophys. J.* 96:19–21.

38. Villalba-Galea, C. A., W. Sandtner, …, F. Bezanilla. 2008. S4-based voltage sensors have three major conformations. *Proc. Natl. Acad. Sci. USA.* 105:17600–17607.

39. Kohout, S. C., S. C. Bell, …, E. Y. Isacoff. 2010. Electrochemical coupling in the voltage-dependent phosphatase Ci-VSP. *Nat. Chem. Biol.* 6:369–375.

40. Ratanayotha, A., M. Matsuda, …, Y. Okamura. 2022. Voltage-sensing phosphatase (Vsp) regulates endocytosis-dependent nutrient absorption in chordate enterocytes. *Commun. Biol.* 5:948.

41. Park, J., D. S. Levic, …, M. Bagnat. 2019. Lysosome-rich enterocytes mediate protein absorption in the vertebrate gut. *Dev. Cell.* 51:7–20.e6.

42. Okamura, Y., Y. Murata, and H. Iwasaki. 2009. Voltage-sensing phosphatase: actions and potentials. *J. Physiol.* 587:513–520.

**Biophysical Journal, Volume *122***

## Supplemental information

# Role of K364 next to the active site cysteine in voltage-dependent phosphatase activity of Ci-VSP

**Ian Costa Paixao, Natsuki Mizutani, Makoto Matsuda, Rizki Tsari Andriani, Takafumi Kawai, Atsushi Nakagawa, Yoshifumi Okochi, and Yasushi Okamura**

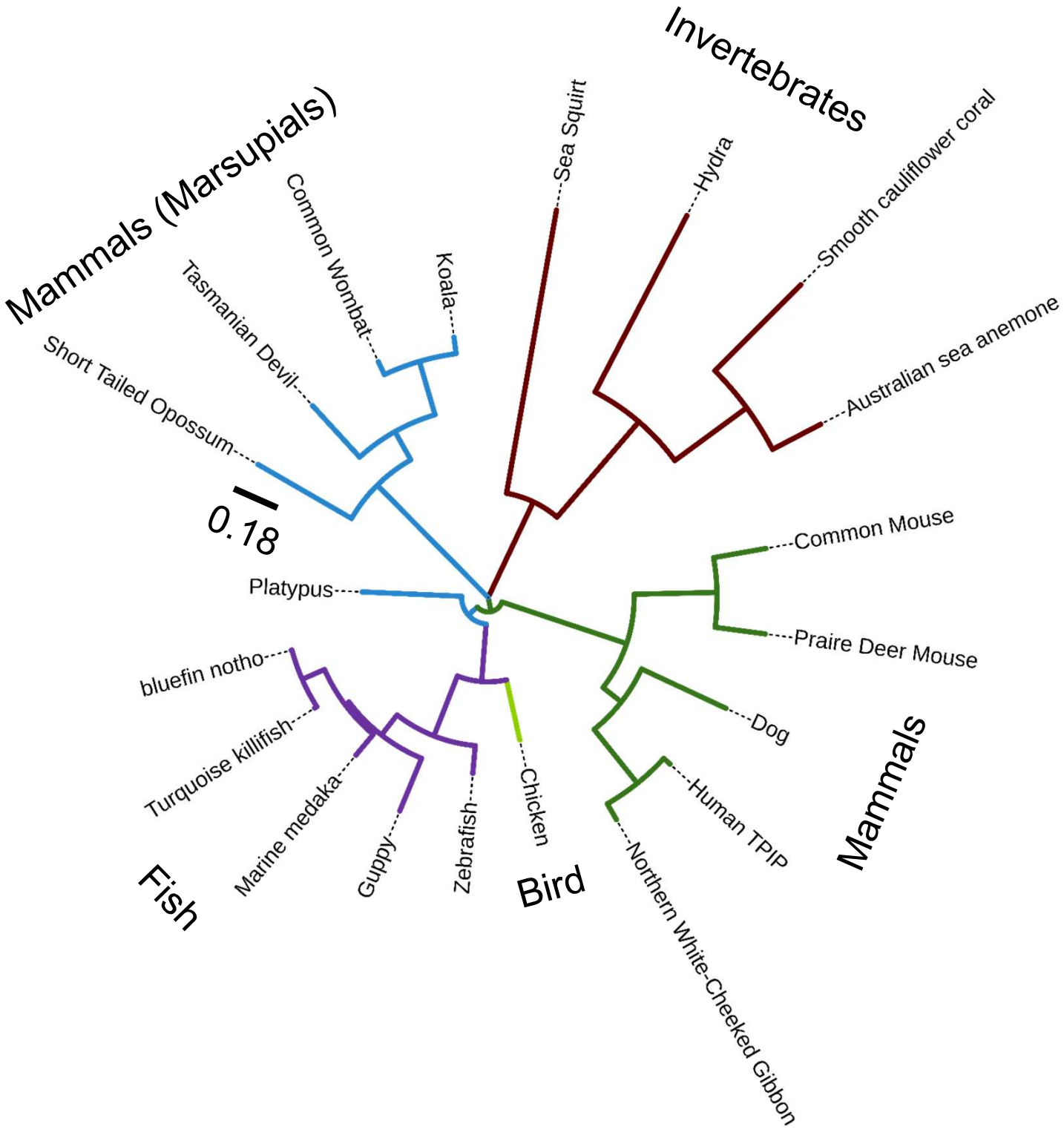


**Figure S1. Phylogenetic tree of mammalian VSP orthologs.**

Phylogenetic tree of VSP orthologs constructed by maximum likelihood test with MEGA 11. Tree is divided in marsupials/mammals in blue, other mammals in green, invertebrates in brown, birds in light green, and fish in purple. Black bar with value is distance scale.

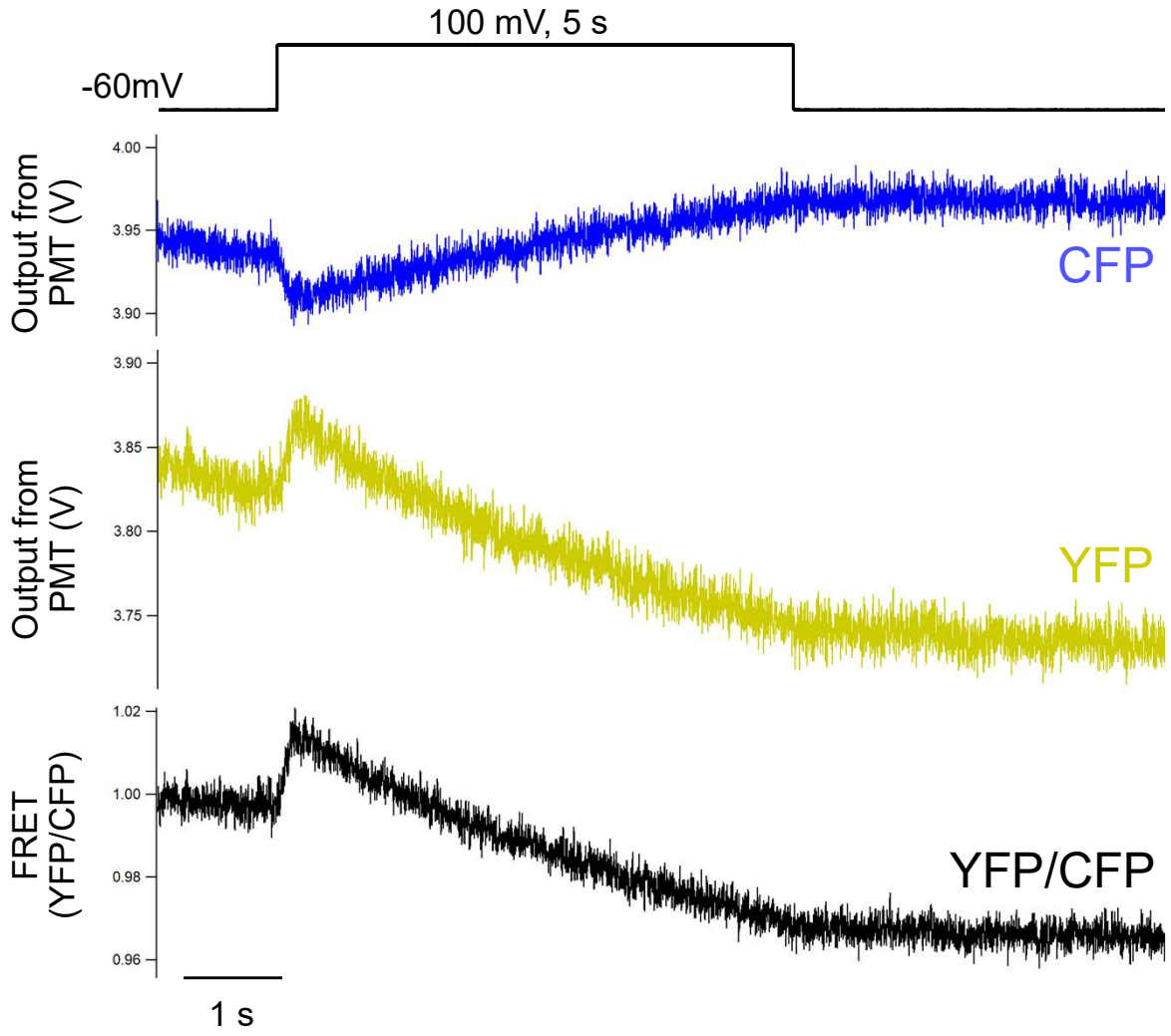


**Figure S2. Raw trace of CFP, YFP, and YFP/CFP ratio signals of F-TAPP probe.**

Representative fluorescence traces of CFP, YFP, and YFP/CFP ratio of F-TAPP recorded from an oocyte expressing WT Ci-VSP upon a depolarizing step to 100 mV for 5 s. Y axis indicates volt of PMT output (CFP and YFP) and ratio (YFP/CFP).

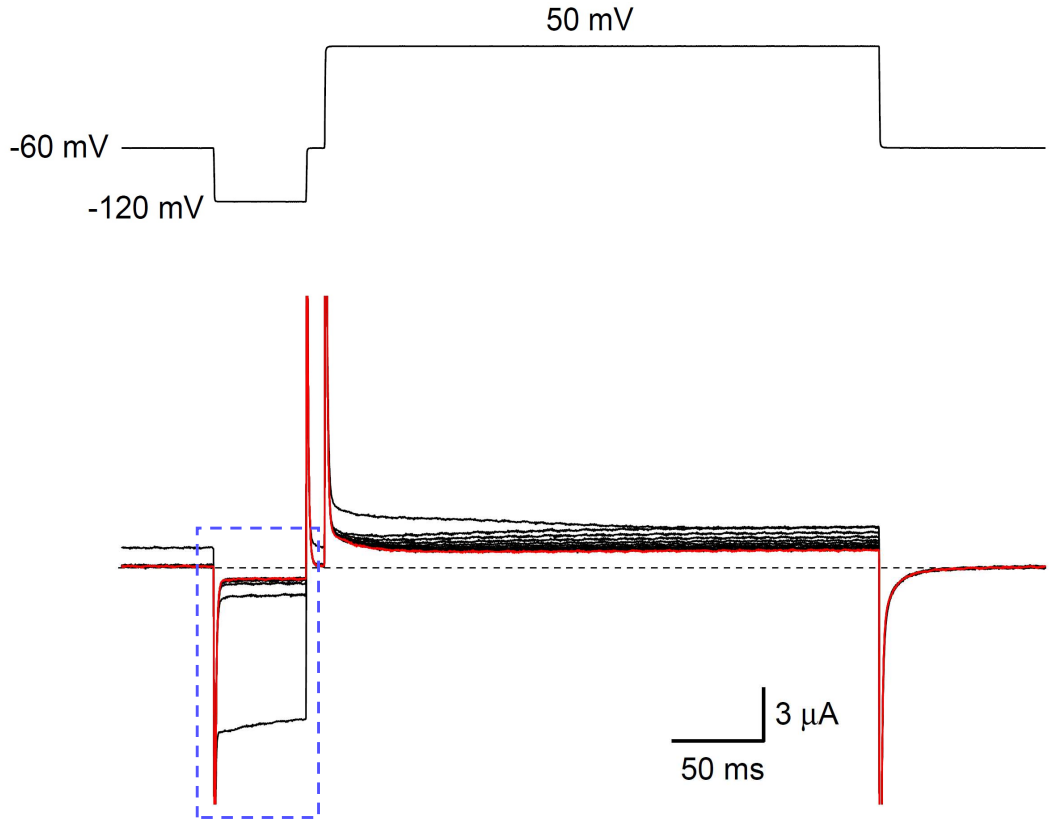


**Figure S3. Protocol to record GIRK2 current.**

Representative GIRK2 current traces in an oocyte expressing WT Ci-VSP (*Bottom*). The pulse protocol (*Top*) composed of a 50-ms test step to -120 mV and 300 ms depolarization (50 mV) was repeated 12 times, and all traces are superimposed. The 12th trace is shown in red. Black dotted line indicates zero current level. Currents recorded during the test pulse (surrounded by a blue dotted square) are shown in Figs. 2*F*, 5*A*, and S4*B*.

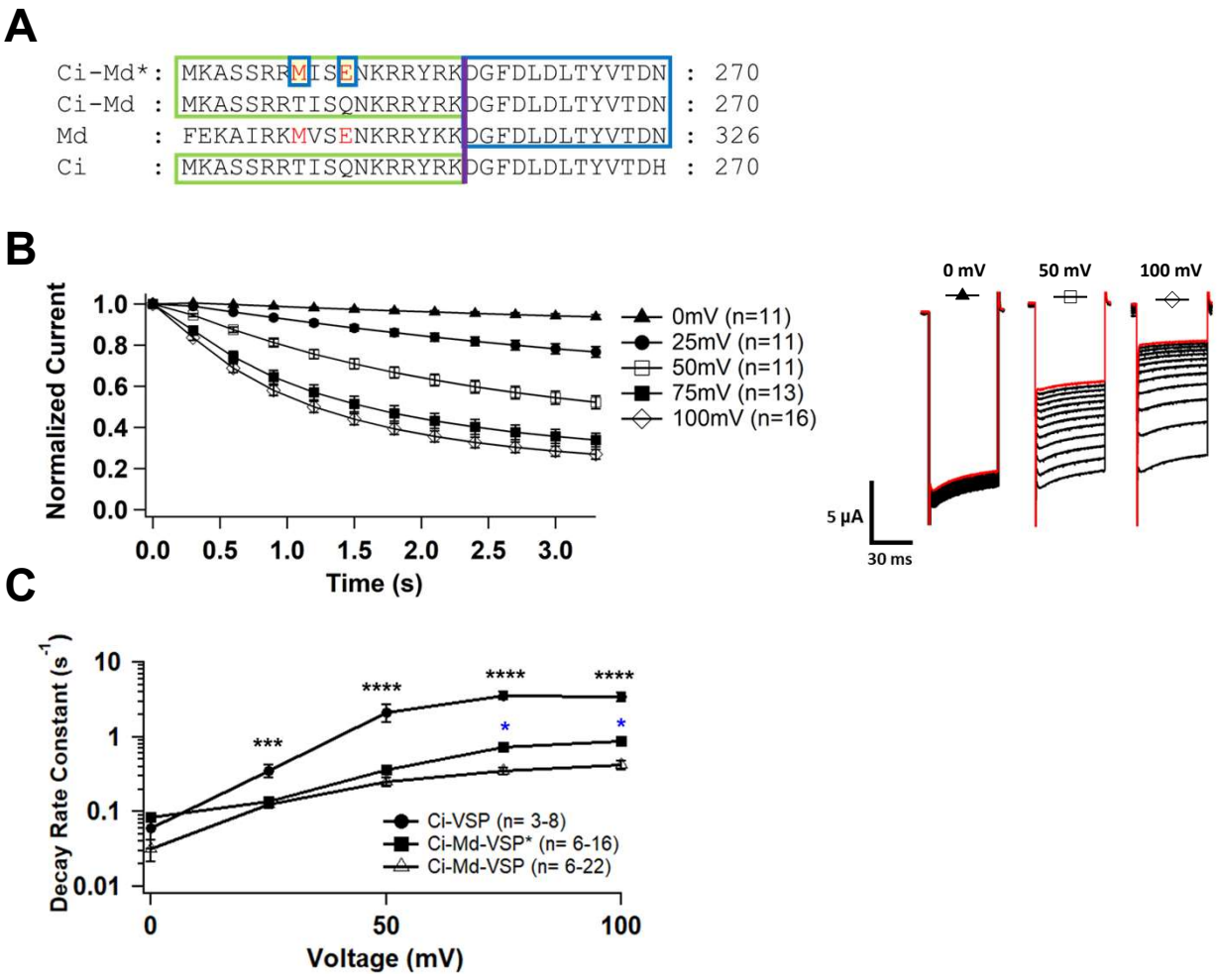


**Figure S4. Characterization of voltage-dependent phosphoinositide phosphatase activity of the *sea squirt-opossum* VSP chimera, Ci-Md-VSP* with the additional mutation of T247M/Q250E in *Xenopus* oocyte.**

(*A*) Amino acid sequences around the junction region of chimeric construction between Ci-VSP; Ci-Md-VSP; and Ci-Md-VSP*. Double mutation of T247M/ Q250E is highlighted in blue. (*B*) Decline time course of Kir current upon voltage-evoked Ci-Md-VSP* activities with five levels of conditioning depolarization (*left*) and the representative raw traces upon -120 mV step with conditioning depolarization to 0 mV, 50 mV and 100 mV (*right*). Data are presented as mean ± standard error (SE). (*C*) Decay rate constant of normalized GIRK2 current at different potentials. GIRK2 was co-expressed with Ci-VSP; Ci-Md-VSP; or Ci-Md-VSP*. * p< 0.05, *** p< 0.001, **** p< 0.0001, one way ANOVA with Tukey's multiple comparisons test. Data are presented as mean ± standard error (SE).

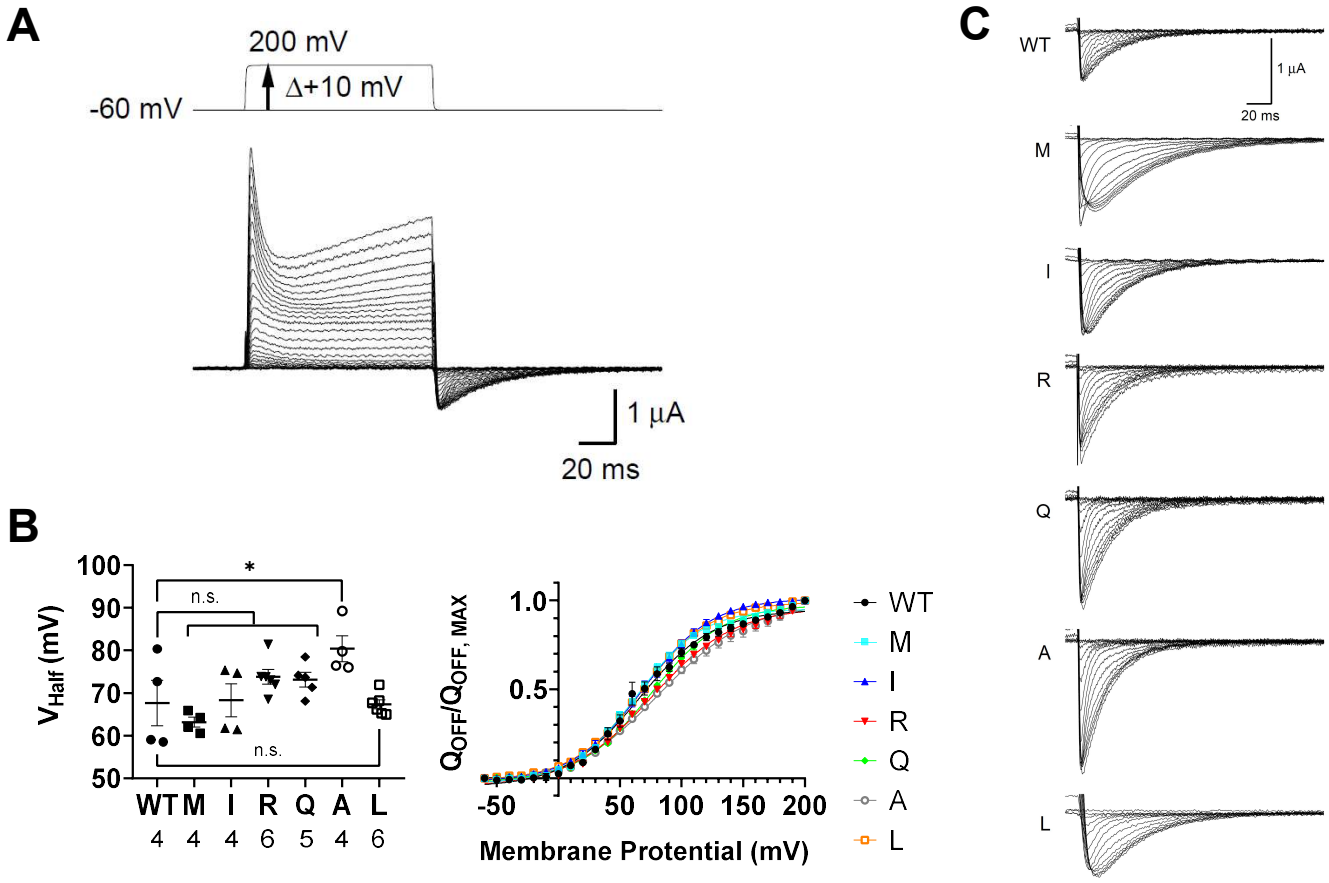


**Figure S5. Sensing current recording suggests similar levels of surface expression and small voltage shift between mutants.**

(*A*) Representative sensing current traces of WT Ci-VSP evoked by depolarizing steps (top). (*B*) $V_{Half}$ (*left*) and $Q_{OFF}$-*V* curve (*right*) of each mutant and Ci-VSP WT. The sensing currents were measured from cells expressing VSP alone and were evoked by depolarizing steps from the holding potential of -60 mV to 200 mV in 10-mV increments. Leak subtraction was performed using a P/-4 protocol. The maximum charges of Off-sensing current ($Q_{OFF}$) was calculated by integration of the off-sensing current which extends 150 ms from the end of depolarizing step. $Q_{OFF}$ was normalized by the maximum charge ($Q_{MAX}$) and plotted against pulse voltage. $Q_{OFF}$-V curves were fitted with the Boltzmann equation: $Q_{OFF}(V)/Q_{MAX} = 1/[1 + exp(-ZF(V-V_{Half})/RT)]$, where *F* is Faraday constant, *R* is the gas constant, *T* is the absolute temperature, *Z* is the effective valency, V is voltage, and $V_{Half}$ is the voltage that gives half of the maximum $Q_{OFF}$ ($Q_{MAX}$). Data are presented as mean ± standard error (SE). * $p<0.05$, n.s.; statistically not significant, one way ANOVA followed by Dunnett's test. (*C*) Representative off-sensing current traces measured by the protocol shown in (*A*). Traces are shown every 20-mV increment.

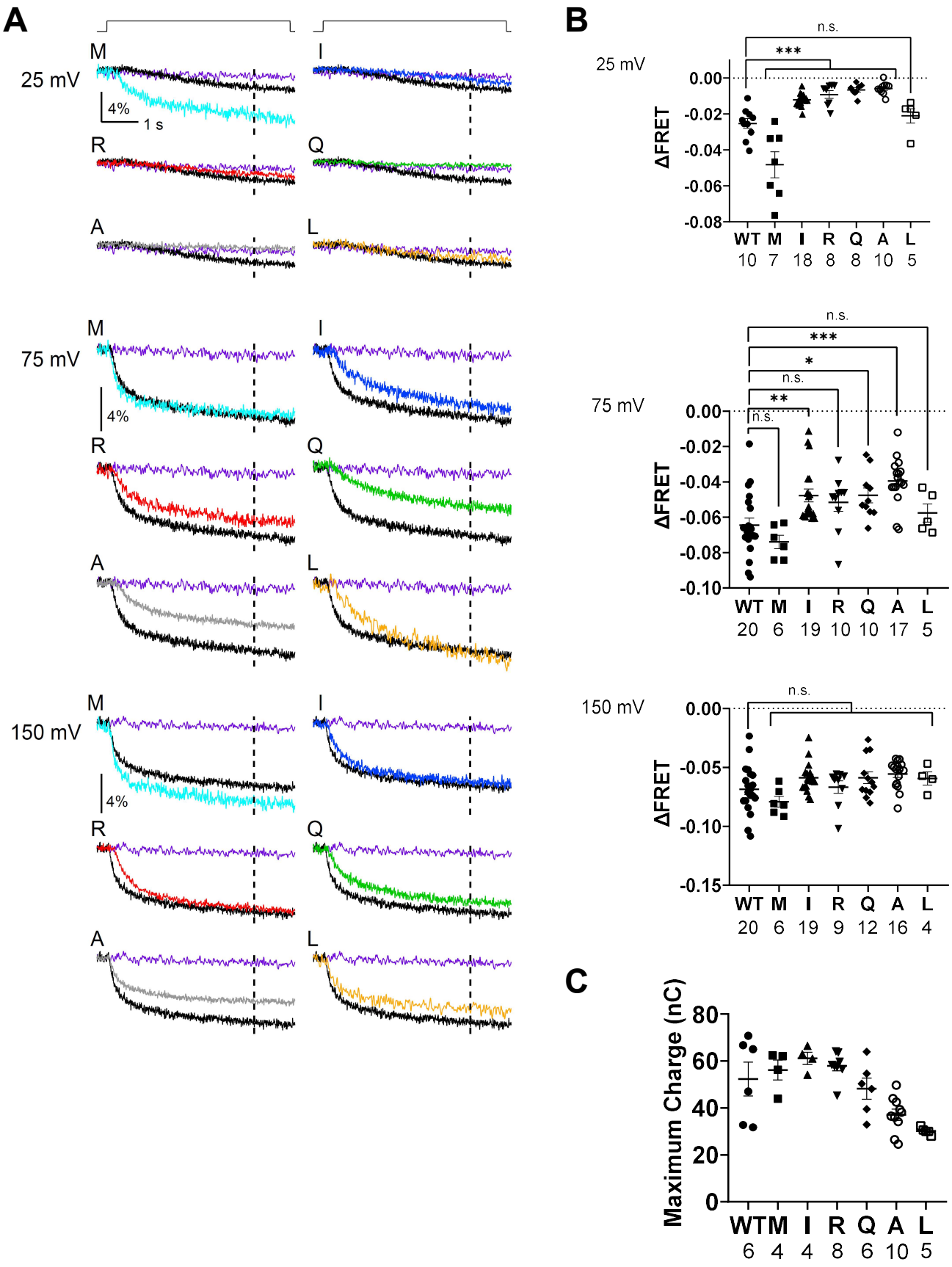


**Figure S6. Voltage-dependent change of FRET signal of PI(4,5)$P_2$-sensing probe, F-PLC, coexpressed with K364 mutant Ci-VSPs in *Xenopus* oocyte.**

(*A*) Representative traces of F-PLC YFP/CFP ratio signal measured at 25 mV (*Top*), 75 mV (*Middle*), and 150 mV (*Bottom*); Depolarizing step shown in top of traces was applied from a holding potential of -60 mV to indicated value for 5 seconds. Dotted line in each trace indicates the time point (at 4 s after the beginning of depolarization) for calculating ΔFRET. (*B*) FRET signal change from the resting level measured at 4 s after initiation of voltage step. Each trace from 0 to 150 mV was obtained from the same oocytes. Data are from the same set as in Fig.4 (0, 50, 100 mV) and complementary to each other. Data are presented as mean ± standard error (SE). * p<0.05, ** p<0.01, *** p<0.001, n.s.; statistically not significant, one way ANOVA followed by Dunnett's test. (*C*) Maximum moving charges calculated from Off-sensing currents at 160 mV, representing cell surface expression level. Data are presented as mean ± standard error (SE).

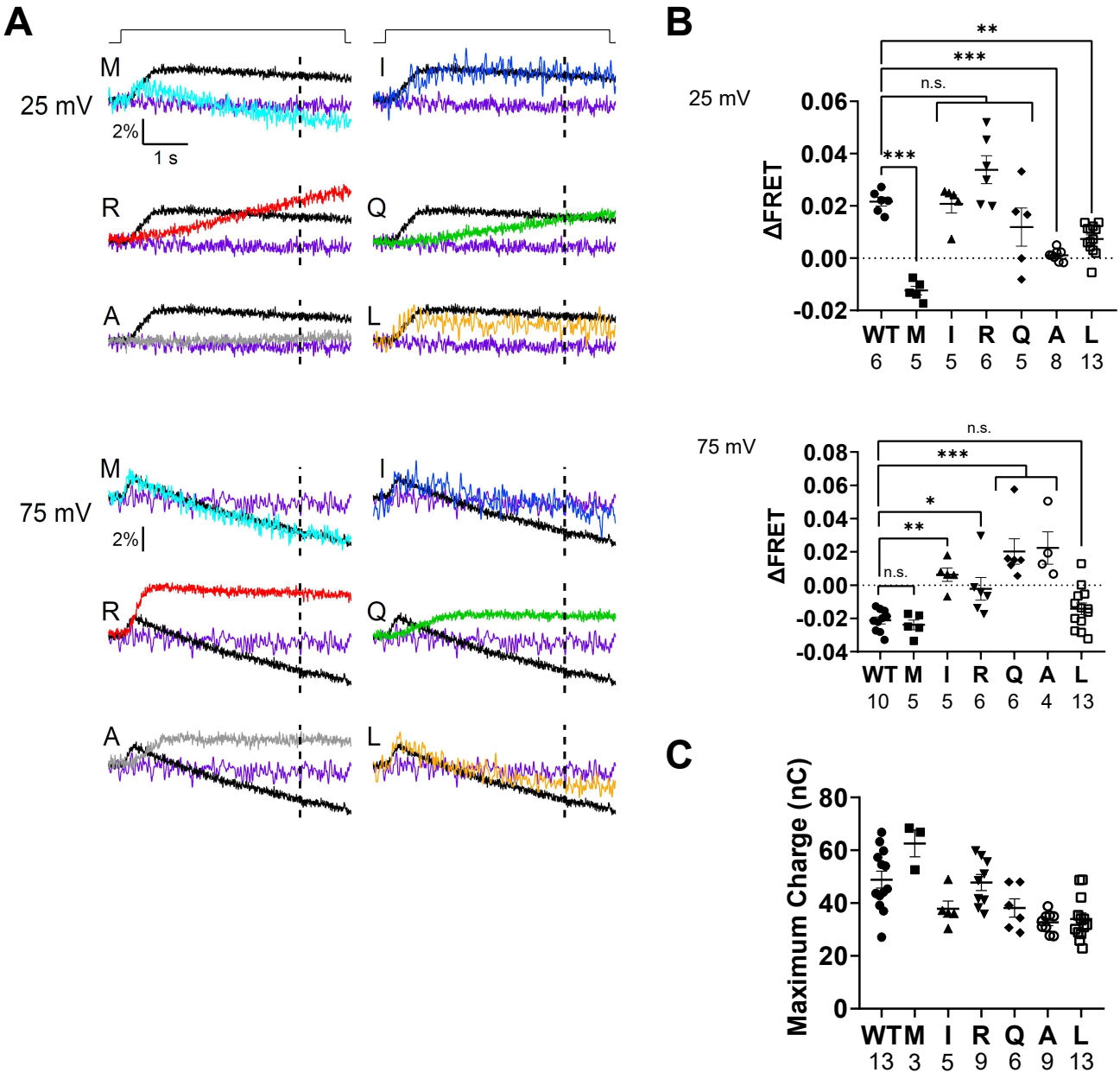


**Figure S7. Voltage-dependent change of FRET signal of PI(3,4)$P_2$-sensing probe, F-TAPP, coexpressed with K364 mutant Ci-VSPs in *Xenopus* oocyte.**

(*A*) Representative traces of F-TAPP YFP/CFP ratio signal measured at 25 mV (*Top*) and 75 mV (*Bottom*); Depolarizing step shown in top of traces was applied from a holding potential of -60 mV to indicated value for 5 seconds. Dotted line in each trace indicates the time point (at 4 s after the beginning of depolarization) for calculating ΔFRET. (*B*) FRET signal change from the resting level measured at 4 s after initiation of voltage step. Each trace from 0 to 150 mV was obtained from the same oocytes. Data are from the same set as in Fig.6 (0, 50, 100, 150 mV) and complementary to each other. Data are presented as mean ± standard error (SE). * $p<0.05$, ** $p<0.01$, *** $p<0.001$, n.s.; statistically not significant, one way ANOVA followed by Dunnett's test. (C) Maximum moving charge calculated from Off-sensing currents at 160 mV, representing cell surface expression level. Data are presented as mean ± standard error (SE).

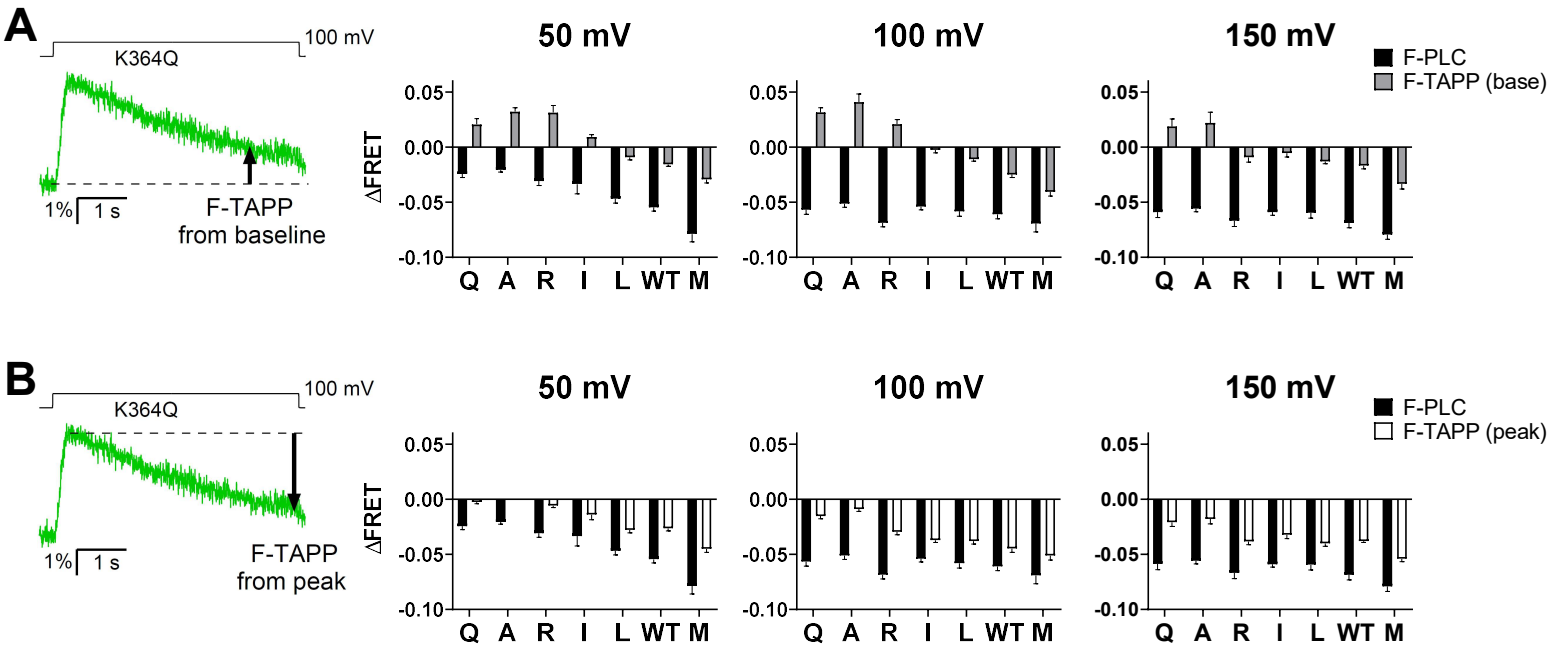


**Figure S8. Summary of $PI(3,4)P_2$ versus $PI(4,5)P_2$ phosphatase activity of Ci-VSP K364 mutants and wild type.**

Graph showing voltage dependent signals of F-TAPP FRET from the baseline for (A) or from the peak for (B) with F-PLC FRET representing $PI(4,5)P_2$ phosphatase activity (subreaction from $PI(4,5)P_2$ to PI(4)P (Fig. 2*A*)). Data for F-PLC FRET in B is the same as in A. Data for membrane depolarization to 50, 100 and 150 mV are presented as mean ± standard error (SE). Sample size is described in Fig. 4*B* and S6*B* for F-PLC, and in Fig. 6*B* for F-TAPP.

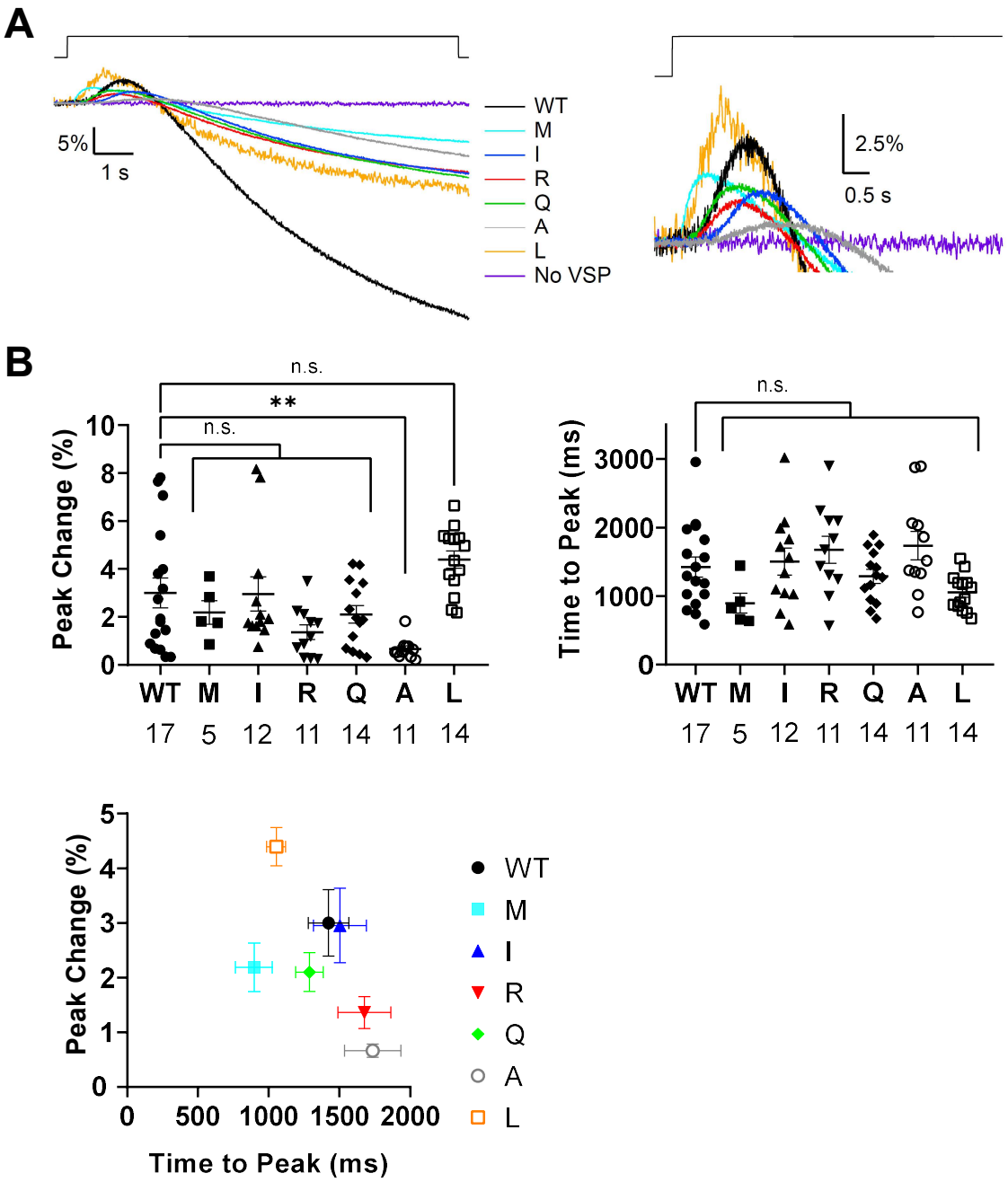


**Figure S9. Comparison of subreaction of 3-phosphate dephosphorylation from PI(3,4,5)$P_3$ among WT and K364 mutants using $PH_{PLC\delta}$-GFP as probe for PI(4,5)$P_2$.**

(*A*) Representative fluorescence traces of $PH_{PLC\delta}$-GFP from insulin-pretreated oocytes. Depolarizing step shown in top of traces was applied from a holding potential of -60 mV to 50 mV for 10 seconds. Magnification of traces at the beginning of depolarization is shown in the right panel. (*B*) *Top*: Peak amplitude of transient fluorescence increase (*left*) and time to reach the peak from the beginning of depolarization (*right*) in WT and K364 mutants. *Bottom*: Peak amplitude vs time to reach the peak for each mutant. Data are presented as mean ± standard error (SE). ** p<0.01, n.s.; statistically not significant, one way ANOVA followed by Dunnett's test.